DETECTING SMALL BURNED AREAS IN THE NETHERLANDS THROUGH SENTINEL-2 DATA

Mariana Diniz Silvestre

Supervisors
Cathelijne Stoof
Harm Bartholomeus

Dissertation submitted for the degree of
Master of Science in
Earth and Environment

July, 2021

WAGENINGEN
UNIVERSITY & RESEARCH

Detecting Small Burned Areas in the Netherlands through Sentinel-2 Data

Mariana Diniz Silvestre

Master Thesis - SGL-80436

July, 2021

Wageningen, The Netherlands

Master's Program	Earth and Environment
Chair Group	Soil Geography and Earth Surface Dynamics
Supervisors	Cathelijne Stoof
	Harm Bartholomeus

Cover page: Sentinel-2 image from Deurnese Peel from 20/04/2020 and image from fire 2018_0214 in Wedde from 30/06/2018. (Source: http://www.dvhn.nl/groningen/Brand-op-akker-bij-Wedde-is-uit-23327176.html)

ACKNOWLEDGMENTS

Sentinel-2 image from Keukenhof region on 22 April 2020.

"An understanding of the natural world is a source of not only great curiosity, but great fulfilment."

Sir David Attenborough

Image from fire 2018_0817 in Molenhoek from 31/08/2018. (Source: http://www.degroesbeek.nl/regionaal-nieuws/95959/grote-heidebrand-molenhoek-forse-schade/)

ABSTRACT

The occurrence and extent of wildfires can be mapped and quantified using satellite imagery. This approach provides quick and standardized detection of burned areas, delivering information even in remote areas. NASA's MODIS sensor onboard the Terra and Aqua satellites is the main source of fire detection for several fire monitoring platforms. However, its main disadvantage is the coarse spatial resolution (250-500m) which limits the recognition of small burned areas (<100 ha). In 2018, MODIS detected only 3 wildfires in the Netherlands, while 949 occurrences on the ground were recorded in the same period. A possible alternative to this problem is the use of Sentinel-2 from the European Space Agency, which has a high spatial resolution (10 to 60m). Therefore, this research aimed to study whether Sentinel-2 data are efficient to detect small burned areas in the Netherlands. According to the Separability Index (M), the NBR (Normalized Burn Ratio) presented the best response for recognition between the NDVI (Normalized Difference Vegetation Index) and BAIS2 (Burned Area Index for Sentinel-2). Due to the inaccuracy of field data, the methodology known as two-phase was applied, using pre- and post-fire images to detect the fire. Furthermore, this method also shows the severity of the fire, which is one of the main factors for burn scar recognition, being even more decisive in fire detection than the size of the burned area. Despite the large presence of clouds and the inaccuracy of field data, this research sees the use of Sentinel-2 as very promising for the study of Dutch fires. This satellite can become a powerful ally helping the country to understand and develop better mitigation strategies for this environmental risk.

Keywords: Small burned areas, Wildfires, Sentinel-2, Spectral indices, the Netherlands

v

Image from fire 2019_0032 in Beekakkersweg from 10/04/2019. (Source: https://www.ed.nl/dossier-112-en-misdaad/boer-ondersteunt-brandweer-bij-blussen-van-bosbrand-in-lage-mierde~aec18356/?referrer=https%3A%2F%2Fwww.google.com%2F)

CONTENTS

TABLE OF FIGURES

APPENDIX

1. INTRODUCTION AND RELEVANCE

Large wildfires around the globe are often reported in the main media because they can cause prolonged consequences and losses for the eco-diversity, human lives and can also impact the economy (Khabarov et al., 2016). Despite its recognizable risk among diverse systems, large wildfires occur much less frequently when compared to small wildfires (Roteta et al., 2019), and therefore, better fire management could be drawn if these small wildfires are mapped (Belenguer-Plomer et al., 2019).

A milestone for the development of the detection and mapping of vegetation fires was achieved with the NASA launch of the Moderate Resolution Imaging Spectroradiometer, known as MODIS on board of Terra and Aqua satellites in 1999 and 2002 respectively (Meng et al., 2015). According to Hantson et al. (2015), MODIS products became widely used by diverse global agencies due to their recognized temporal and spatial consistency to study and monitor fire occurrences. However, there are still some limitations on MODIS use, and the main one is the coarse spatial resolution that the sensor offers (Artés et al., 2019).

In the year of 2018, the Netherlands faced an intensive drought period resulting in a total of 949 wildfires, approximately 3 times more wildfires registered than the year before (San-Miguel-Ayanz et al., 2018). However, only 3 occurrences of these total were detected by the MODIS satellite (San-Miguel-Ayanz et al., 2018). This shows that most wildfires in the country are occurring below the detection limit for the current products that European Forest Fires Information System - EFFIS provides. Figure 1 represents the EFFIS data detected through the MODIS satellite for the Netherlands and in comparison, with data obtained on field.

Figure 1: Contrast between the EFFIS data obtained through MODIS satellite for the Netherlands and the data collected on field.

These numbers prove the clear underestimation of the numbers of wildfires identified through MODIS and go in accordance with Boschetti et al. (2009) who declare that the spatial resolution significantly impacts the accuracy for mapping burned areas.

Recent studies have shown that the efficient mapping of small burned areas holds a great impact on the total number of MODIS products, and in some cases, the underestimation of the mapped regions can reach almost 45% of the total mapped areas (Roteta et al., 2019). This represents a considerable implication given the fact that smaller fires can be as destructive as larger wildfires and they normally occur close to urban clusters (Randerson et al., 2012). The small wildfires can provoke even more serious consequences in places such as the Netherlands due to its large populational density and low awareness and preparedness to handle such events (Stoof, personal communication, 2020).

Therefore, detecting and mapping small burned areas is of great importance for risk management. This opens opportunities to study fire behaviour in a specific region, helping to create more efficient management services, better fire preventive measures, and effective land management (Camia et al., 2014; Tedim et al., 2015). Besides, the information obtained can be used to carry out risk assessments of affected and surrounding areas, and the spatial data collected over time can be used to monitor environmental recovery, especially concerning to agriculture, which is a very important sector for the Dutch economy.

Aiming an improvement in the identification of small wildfires, studies based on the products of the Sentinel-2 can be applied to perform the recognition of smaller burned areas (Roteta et al., 2019; Weirather et al., 2018), since this satellite provides images with a high spatial resolution (10m, 20m, and 60m depending on its spectral bands). If the detection of the small burned areas is efficient with Sentinel-2, this research may indicate possible advancements and limitations within this type of study in the Netherlands gathering more information over wildfires. This can have significant importance considering that the Netherlands Fire Service did not collect any data since 1996, returning the practice in 2017 (Stoof, personal communication, 2020).

2. RESEARCH OBJECTIVES AND HYPOTHESIS

Understanding the importance of accurate mapping of small burned areas to strengthen the knowledge and support fire management to protect ecosystems and human population, this research has the main objective to identify small burned areas in the Netherlands through Sentinel-2 imagery collected in the years 2017-2019. Hence, the main research question is:

Can small burned areas in the Netherlands be identified using Sentinel-2 data?

To guide the central objective, the following sub-questions are raised, and some hypotheses are brought:

- *Which of the applied spectral index has the best response for detecting small wildfires?*
Roteta et al. (2019) developed a Sentinel-2 burned area algorithm to identify small burned areas for sub-Saharan Africa with satisfactory results by using common spectral indices that cover the Visible, the Near Infra-Red (NIR), and Shortwave Infra-Red (SWIR). Thus, using spectral indices such as Normalized Difference Vegetation Index (NDVI) and Normalized Burned Ratio (NBR) are seen in the current research as promising applications.
In addition, a spectral index developed by Filipponi (2018), the Burned Area Index for Sentinel-2 (BAIS2), is being progressively applied in this field with great efficiency as seen in Filipponi (2019), Lasaponara et al. (2020), Brovkina et al. (2020), Smiraglia et al. (2020) and van Dijk et al. (2021).

Therefore, this research positively believes that it will be possible to identify small burned areas the Netherlands?

- *Will the identification of small burned areas be efficiently performed outside of the fire season?*

This is a bottleneck for the research, because one of the possible limitations is to find images cloud-free, and the Netherlands is known for its cloudy and rainy weather. The application of cloud masks in the images can cause shadows in the terrain, which may influence the results. In addition, researches usually investigate wildfires that occur during the dry season, which in many cases represents a favourable condition for this type of event and, when plants are still in an active photosynthetic state. Likewise, most studies on wildfires focus on Tropical and Mediterranean climates, but it is known that the results may be different in other season conditions.

- *How long after a fire has occurred can it still be detected?*
    - *Does this depend on the size and/or severity of the wildfire?*

This question can bring some insights over the detection, knowing that finding images right after the fire event can be a difficult task. Eventually, the interval between the date of the fire event and the date of the image may result in a sufficient time for recovery (even if partial) of the land cover. Besides, the time for the detection can also be related to the severity of the fire. According to Certini (2005), severity is the relationship between temperature peaks and fire duration, therefore, this research assumes that fire severity can influence the detection of fire scars; the more severe the fire, the more evident the scar that can result in slower vegetation recovery. And the same idea is given by the size of the area, the larger the burned area, the longer the recovery time.

3. BACKGROUND

3.1 Wildfires in Europe

Wildfire is a natural phenomenon where the vegetation plays the role of the main fuel for this combustion, and many ecosystems have adapted to perform better in this extreme circumstance and depend on it for renewal and maintenance (Khabarov et al., 2016). On the other hand, wildfires can become an uncontrollable fire threatening terrestrial ecosystems and human lives (Moritz et al., 2012).

In general terms, wildfires are an emerging problem all over the world, occurring mainly in tropical forests and savannas in Africa, Indonesia and Brazil, in grassland and temperate forests in South America, the USA and Eurasia, as well as in the boreal forest in North America and Siberia (Chuvieco et al., 2018). Albeit some evidence, the interplay between fire and climate regimes are not yet fully understood, however, it is evident their mutual effect (Chuvieco et al., 2018).

Hawthorne and Mitchell (2018) state that the increase in the frequency and severity of these wildfires seen in the past decade are positively related to global warming, and northern European countries that have not been concerned with wildfires in the past, are seeing the signs of this new threat. An example is worth mentioning is Sweden, which in 2014 faced a large and unexpected wildfire that consumed around

15000 ha (Tedim et al., 2015). A similar trend is also observed in other northern European countries such as the United Kingdom, Norway, and the Netherlands (Flannigan et al., 2013).

In addition to the possible relationship with global warming, the rise in the number of wildfires has a clear correlation with the increase in population density. The growth of urban expansion in the wildland-urban interface (WUI) and changes in land-use practices that conflict with social and ecological protection in Europe, help to increase the risk of fires (Tedim et al., 2015). Wildfires can transform landscapes and ecosystems and, in general terms, the continent has more than 65000 occurrences of forest fires annually, totalling about 4 million km^2 of burnt area (San-Miguel-Ayanz et al., 2018), diminishing the carbon stock of forests and soils, which can cause loss of life and economic problems (Bowman et al., 2009; Marlier et al., 2013).

Despite the European countries having a clear history of using fire in agriculture, the quantity and the quality of information are deficient when there is a comparison among the countries, which brings uncertainties for the studies (Camia et al., 2014). There are disparities between data from Mediterranean countries with some Western and Northern European countries because the Southern countries such as Portugal, Spain, Greece, and Italy have a significant historical context for wildfires.

A complete and solid fire dataset that contains not only the location of the fires but also their cause can help the understanding of the fire behaviour for better management and control of wildfires. Moreover, mapping wildfire risks and vulnerabilities can support the development of fire prevention policies through the identification of Wildland-Urban Interfaces (WUI) areas (Modugno et al., 2016).

Wildland-Urban Interface represents an area where urban settlements encounter natural vegetation in which there is a favourable possibility of wildfires. Statistically speaking, Wildland-Urban Interface areas are twice as likely to start the fire ignition than no Wildland-Urban Interface areas (Chas-Amil et al., 2013). This is because about 90% of the fires registered globally are due to human activities (San-Miguel-Ayanz et al., 2012; Vilar et al., 2015), which places the Netherlands at a considerable risk of wildfires occurrence (de Vos, 2018).

According to de Vos (2018), the country has many regions that can be classified as Wildland-Urban Interface and represent the 16th most populous nation in the world, and the 5th in Europe (OECD, 2020). This goes in accordance with Smeenk (2011) who states that in the Netherlands the vast majority of wildfires tend to be small, are human-caused, and are easily contained.

After 1996, the Staatsbosbeheer (Dutch forest management) stopped registering the wildfires occurrence and as a result, the Dutch Statistics (CBS Natuurbranden - Centraal Bureau Voor de Statistiek) incorporated natural fire episodes with other types of fire events (Stoof, 2020). In 2017, a full track on the country wildfires was established again through a collaboration between the Netherlands Fire Service, the Institute for Physical Safety and Wageningen University & Research (Stoof, 2020), however, there is still a gap of almost 20 years of information (Stoof, personal communication, 2020).

In addition, for the years that the fires started to be recorded again - 2017, 2018, and 2019 - the unknown causes comprehend sometimes even 50% of the total fire registered (Figure 2) (Stoof, 2020), which still shows gaps in the recently reported fire occurrence. The same happens with the information about the

total area burned. The lack of extensive knowledge about the exact cause of forest fires in the Netherlands represents the deficiency of a basis for well-informed prevention campaigns.
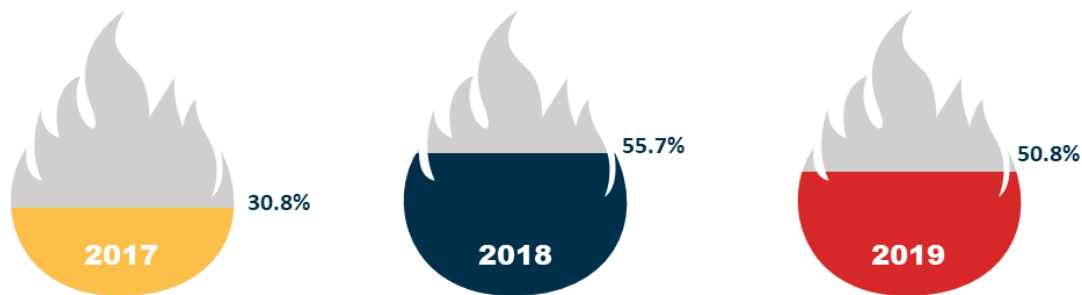
Figure 2: Total of fire occurrences without a known cause.

Likewise, according to Yang et al. (2007), the information on the spatial distribution of wildfires is vital to improve prevention strategies, also because frequent small wildfires can evolve into larger fires. Spatial analysis of events can provide new information to guide planning and risk reduction efforts. An efficient form of prevention/mitigation is given by an effective assessment system made through Earth Observation (Pettinari & Chuvieco, 2020). Doerr et al. (2013) also affirm that the availability of satellite data allows a more efficient evaluation of areas burned, offering a standardized and valuable assessment.

3.2 The use of GIS technologies to study, prevent and mitigate wildfires

Traditionally, information about wildfires used to be collected by government agencies from field estimates by fire management teams. However, the absence of a standard collection among individual countries has led to a questionable source of information on regional, continental, and global scales (Chuvieco et al., 2019). Few years after the launch of the first's satellites in the 1970s decade, satellite imagery became an important source in providing compelling data on fire-affected areas around the globe (Chuvieco et al., 2019).

Assuming the importance and the constant occurrence of wildfires on a global level, Geographic Information Systems (GIS) methods have become a powerful ally to study, understand and fight against this environmental phenomenon. For Huang et al. (2016), the use of satellite data has been systematically employed to monitor wildfires around the globe at coarse resolution, applying algorithms that help to identify active fires as well as to map the spatial extension of the affected areas. However, with the global increase of wildfires occurrence possibly due to climate change, the need for burned area products at a moderate and high spatial resolution is of extreme importance to protecting thousands of people and diverse ecosystems (Weirather et al., 2018).

According to Filipponi (2018), nowadays satellites play a key role in assisting knowledge about wildfires by promoting early information to map burned areas. They provide precise and reliable data, which is fundamental to support fire management, helping to define planning strategies, also accounting for the environmental losses.

This rapid information is provided mainly by the MODIS (Moderate Resolution Imaging Spectro-radiometer) sensors onboard of twin's Terra and Aqua satellites, which have 1-2 days revisit-time. However, the active fire detection products from MODIS, are often neglecting burned area patches, resulting in an underestimation of the area burned. This can be explained by the MODIS coarse spatial resolution, around 250m to 500m (Roteta et al., 2019), which limits the recognition of small burned areas. For this reason, the identification of small wildfires (< 100 ha) using this sensor is a challenging task, especially when it is estimated that globally around 26% of the burned areas that have been recorded, are the result of small fires (Roteta et al., 2019).

After 2015 with the launch of the two Sentinel-2 satellites, the scenario for mapping small wildfires became promising. Sentinel-2 is part of the Copernicus Program developed by the European Space Agency (ESA) to provide environmental services and natural disaster management through the monitoring of the land surface conditions (Roteta et al., 2019). The main advantage of Sentinel-2, composed of two identical polar-orbiting satellites in the same orbit, is its high spatial resolution varying from 10m to 60m, depending on the wavelength given by the Multi-Spectral Instrument (MSI) (Roteta et al., 2019). On the other hand, its disadvantage is the revisit time of 5 days at Equator latitudes (10 days each satellite) and 2 to 3 days at mid-latitudes, compared with the 1 to 2 days revisit cycle from MODIS.

While active fire products capture information about the location and timing of fires burning at the moment that the satellite overpass, e.g. MODIS, they do not generally permit the reliable estimation of a burned area (Giglio et al., 2006). Thus, the efficiency of Sentinel-2 relies on its burned area product given the extent of burn scars over a specified period, being an indispensable tool to assist fire management (Filipponi, 2018).

3.3 Sentinel-2 and the spectral bands

The Copernicus Program was developed by ESA as part of a platform of Earth Observation through the Sentinel Mission to assist environmental matters (monitoring atmosphere, water, and land) and on natural disaster management (ESA, 2015; Roteta et al., 2019). This program has evident importance due to the high data quality, a wide range of Earth Observation capacity, and accessible information, all provided by an open data system catalogue via a central hub (https://scihub.copernicus.eu/).

The main applications of Sentinel-2 (S-2) rely on forest management, land ecosystems, agriculture, and disaster mapping (ESA, 2015), and that is why it was chosen for this research. As mentioned before, Sentinel-2 is a constellation composed of twin Satellites (Sentinel-2A and Sentinel-2B) moving at the same orbit and separated by a distance of 180°. Combined, they generate moderate to high spatial resolution images (60m to 10m) with global coverage of around 5 days.

The sensor responsible for capturing the image is the MSI – MultiSpectral Instrument which is a passive pushbroom detector that assembles the sunlight reflected from the Earth (Roteta et al., 2019). It counts with 13 spectral bands, with wide spectral coverage from the Visible to Short Wave Near Infra-Red (SWIR), and they can be separated according to their spatial resolution (Table 1).

Table 1: Spectral bands for the Sentinel 2A and 2B. Adapted from ESA (2015).

Spatial Resolution (m)	Band Number	Band Name	Sentinel-2A	Sentinel-2B
			Central Wavelength (nm)	Central Wavelength (nm)
10	2	Blue	492.4	492.1
	3	Green	559.8	559.0
	4	Red	664.6	664.9
	8	NIR (Near Infra-Red)	832.8	832.9
20	5	Vegetation Red Edge	704.1	703.8
	6	Vegetation Red Edge	740.5	739.1
	7	Vegetation Red Edge	782.8	779.7
	8a	Narrow NIR	864.7	864.0
	11	SWIR (Shortwave Infra-Red)	1613.7	1610.4
	12	SWIR (Shortwave Infra-Red)	2202.4	2185.7
60	1	Coastal Aerosol	442.7	442.2
	9	Water Vapor	945.1	943.2
	10	SWIR - Cirrus	1373.5	1376.9

The advantages of Sentinel-2 go beyond the high spatial and temporal resolution. The 13 bands can support a great enhancement for spectrum analyses. As an example, the three Red Edge bands (bands 5, 6, and 7), plus the narrow Near Infra-red (band 8a) are excellent for vegetation characterization (Smiraglia et al., 2020). This parallel can be better interpreted in Figure 3 that represents a basic Spectral Signature for vegetation, soil, and water.
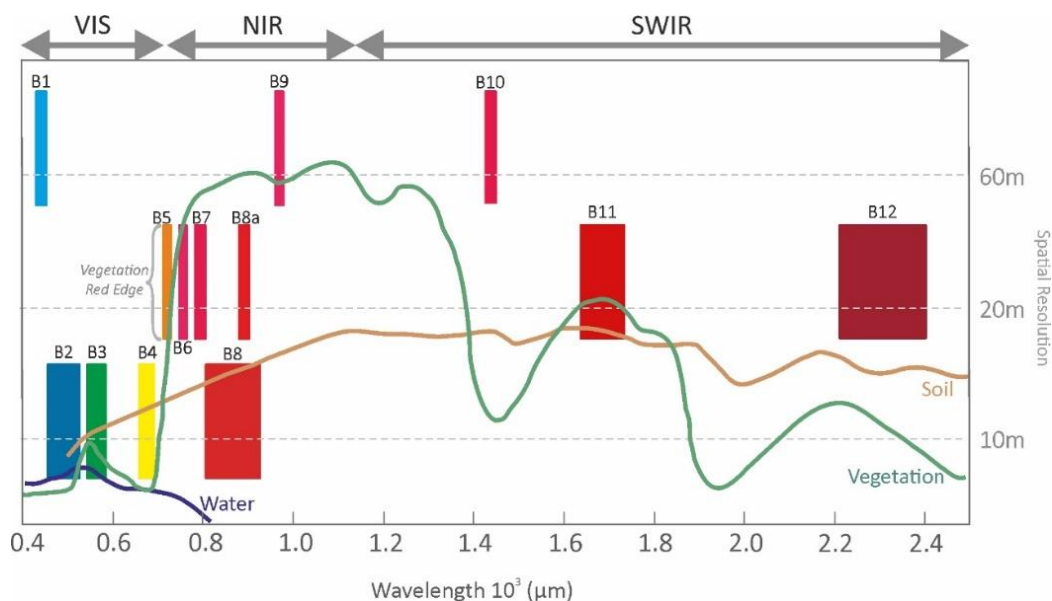
Figure 3: Spectral Signature for vegetation, soil, and water with the spectral bands from Sentinel-2. Adapted from Huete (2004) and ESA (2015).

This image helps one to understand the following conclusion: in a green healthy plant, the chlorophyll absorbs a large proportion of red and blue spectrum and reflects in the green. It also presents lower reflectance in the shortwave infrared (SWIR) influenced by the water content, which absorbs infrared energy (Figure 4).
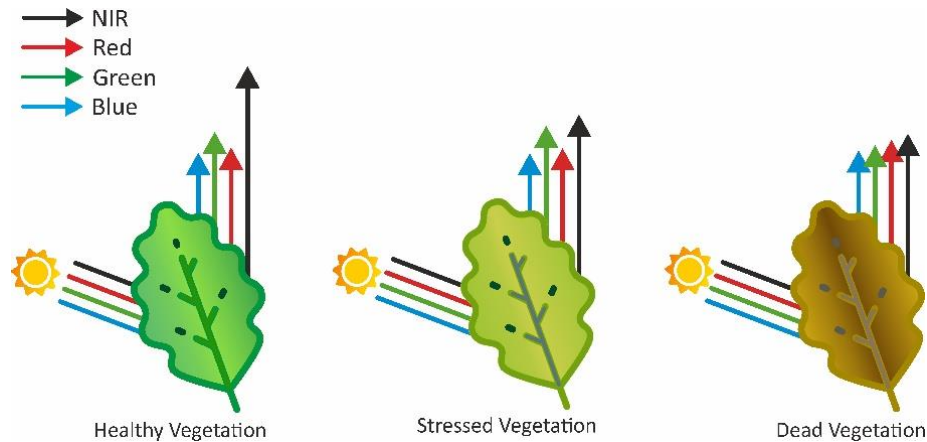
Figure 4: Representation of spectral vegetation signatures. Adapted from Jupudi (2018).

And therefore as a general rule, spectral indices for vegetation can be based on the concept that healthy vegetation will reflect in the NIR – near-infrared in the optical spectrum and absorbing in the visible red (Jupudi, 2018).

Additionally, Bastarrika et al. (2014) showed that the near-infrared (NIR) in the spectral region, the signal for burned areas is highly sensitive, being in a favourable range for mapping wildfires. Schroeder et al. (2016) described that the pre-fire images of an area generally depict high reflectance in the NIR range, while there is a decrease in reflectance in the post-fire scenario. Thus, the combination of specific bands can result in more suitable spectral indices for the detection of burned areas.

4. METHODOLOGY

4.1 Description of the study region

This study focuses on the Netherlands, located in Western Europe, and the main country from the Kingdom of the Netherlands. It is known for its extremely flat landscape and approximately half of the territory is located 1 meter above sea level. According to the Organization for Economic Co-operation and Development (OECD, 2020), in 2018 the Dutch population was around 17.2 million people, making it one of the most populated countries in the world with a population density of 488 people per km^2.

Although not as affected by fires as other European countries, such as Portugal, Spain, and Greece, which usually face severe fire seasons (Doerr et al., 2013), the Netherlands in 2018 recorded 3 times more wildfire fires than in 2017.

According to San-Miguel-Ayanz et al. (2018), in 2018 the majority of wildfires in the Netherlands occurred in the Veluwe region (located in the centre of the country), Limburg, and Noord-Brabant (both in the southeast region). The fire season occurs mainly in Spring with warm and dry weather.

Figure 5 shows the study area with the burned areas from the EFFIS database detected through the MODIS sensor over 8 years (2011 to 2019) in contrast with the data acquired on the field starting from 2017 to 2019.
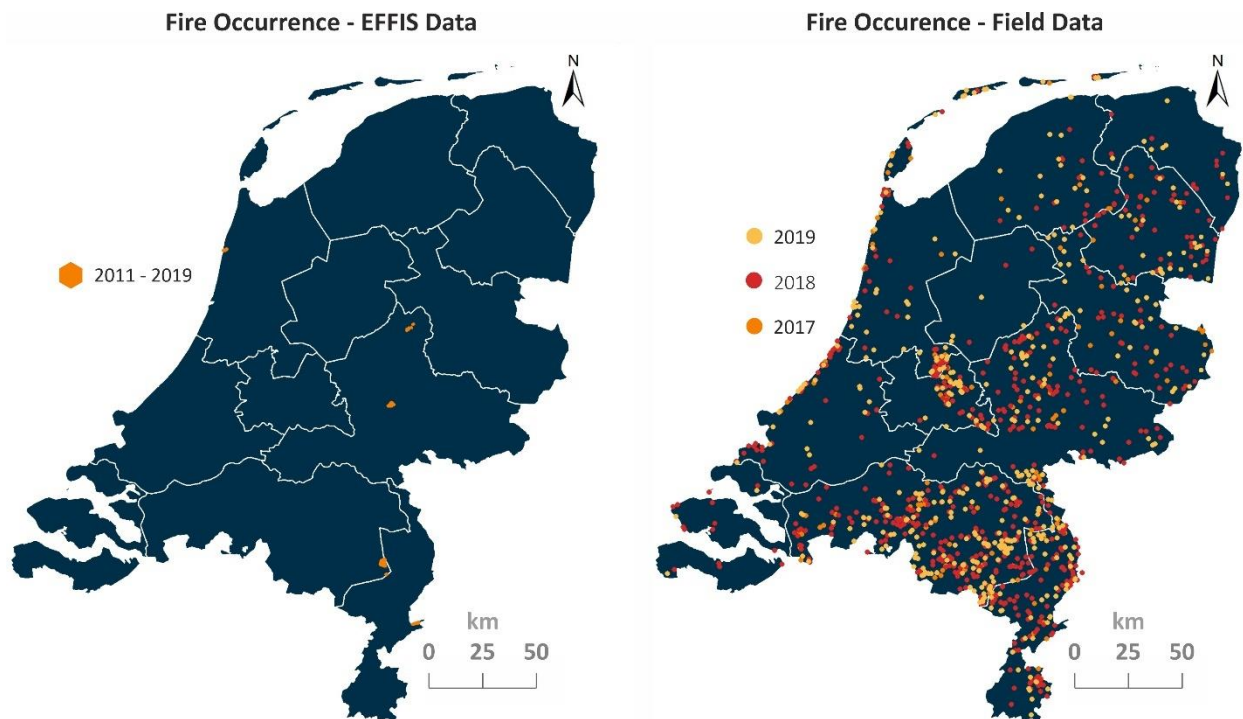
Figure 5: Study area with the burned areas that were recorded in the EFFIS database between the years 2011 and 2019 and the burned areas recorded in the field between 2017 and 2019.

4.2 Data Description

4.2.1 THE NETHERLANDS WILDFIRE DATA

In 1996 the Staatsbosbeheer (the Dutch Forest Commission) interrupted the fire record, and the CBS Natuurbranden (Dutch Central Bureau of Statistics) decided to incorporate natural fire episodes with other types of fire events, which makes it difficult to have clear conclusions about wildland fires. (Stoof, personal communication, 2020).

In 2017, a full track on the country's wildfires was established again through an informal collaboration between the Netherlands Fire Service and the Institute for Physical Safety from Wageningen University & Research (Stoof, 2020). It is important to point out, that despite these reliable records, there are still some imprecisions within the data, such as the absence of coordinates. The fire locations were reported through street names on the surrounds of the event. The coordinates were therefore approximately added based on the street names with the help of an online geocoder (www.gpsvisualizer.com) performed by a previous master's student, Mathu (2020).

Concomitantly, Agricola & Stoorvogel, in 2020 used a similar method was used to add new geographic coordinates in the same data aiming higher accuracy. Using the roads network dataset available at pdok.com, a relationship was made between the location of the road (name of the road and municipality)

and the location where the fire event was reported. Besides, a buffer of 200 meters was defined for a road or road section, so fires located within this area were linked to that particular road, and consequently, to the municipality. Thus, each road section was converted into a point data – located in the centre of the buffer - with x and y coordinates, which was then considered the estimated location of the fire event.

Both sets of data contain the same main information, except for differences in the values of the coordinates. Therefore, it is important to emphasize that there are certain inaccuracies in terms of the exact location of the fire. Altogether, these databases contain information on 1817 wildfires that occurred between 2017 and 2019 with the date, location, cause of the fire, size of the burned area, and type of vegetation (Rooij et al., 2020). An overview of the distribution of fire between months can be seen in Figure 6, where it is possible to see the high number of occurrences in the months of July and August 2018 which is the result of the severe drought that the country went through that year.
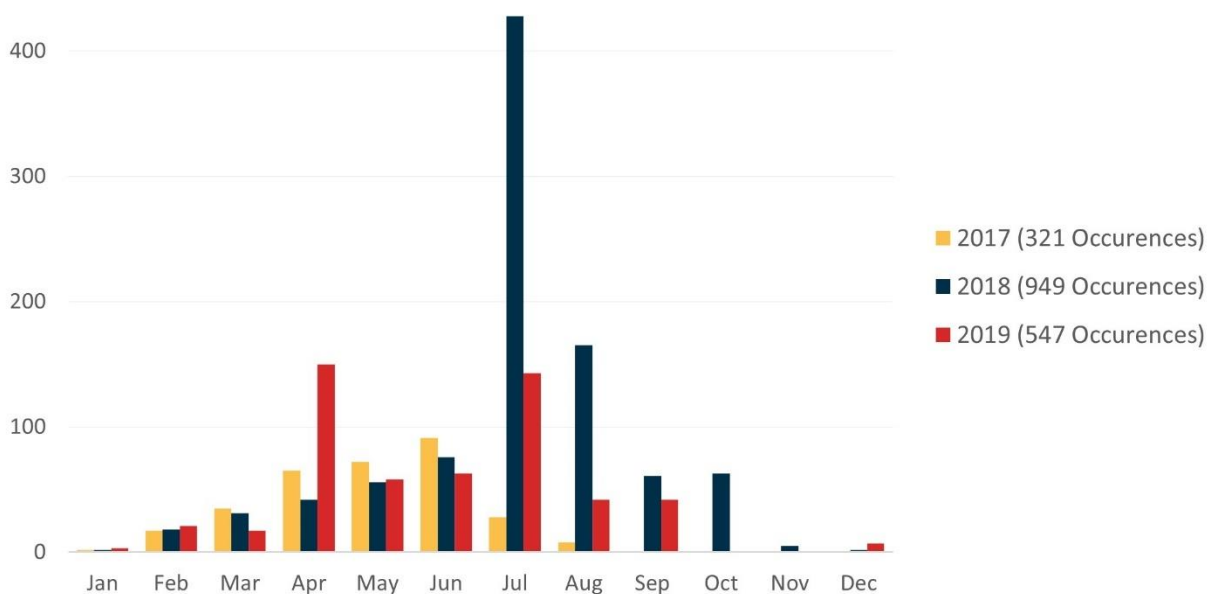
Figure 6: Monthly wildfire occurrence for 2017, 2018, and 2019. Source: the Netherlands Fire Service dataset.

4.2.2 SENTINEL-2 IMAGERY

According to the European Space Agency, all the Sentinels products are open source, therefore are free of charge to all its users and the public thus, anyone can access the Sentinel's images. For this research, an account was created for access to the Copernicus Open Data Hub to obtain the images (https://scihub.copernicus.eu/dhus/#/home).

There are other ways to download the images directly through websites as PEPS, USGS CODE-DE, or through cloud environments, for instance AWS – Amazon Web Services and DIAS platform (Copernicus Data and Information Access Service), and even making use of software such as Python, QGIS and R (one can check an extensive list of options accessing https://github.com/Fernerkundung/awesome-sentinel). All those options offer free access to Sentinel data, however with some constraints. Most of the free

options have a download limit per account and long waiting time to get access to the requested image. Likewise, a number of these options require from the users some programming skills, which can difficult the process (Ranghetti et al., 2020), and also only the most recent images are automatically available for download.

Usually, images are available on average 15 months from the current date. The previous images are removed from the online archive and are only available in Long Term Archives (LTA) and will be accessible again for 48 hours after the user requests one or more LTA recoveries. The entire process of querying an old image can take up to 4 days.

As an alternative, the R software was used to download the images of the present study, which allows the request of up to 50 images at the same time, while through the Copernicus Hub, only 2 are allowed per time. The retriever time can vary from 2 hours to 12 hours.

As standard, Sentinel-2 products are always supplied as a ZIP file in SAFE format (Standard Archive Format for Europe) and each of these files contains surface reflectance information stored as a JPEG2000 multispectral raster being represented on 100 x 100 km tiles from the Sentinel -2 global grid (ESA, 2015; Ranghetti et al., 2020).

The main input data for the present study was the Level-2A product characterized by tiles of 10000 km^2 rectified images based on the UTM/WGS84 projection. This product is already atmospherically corrected to mask defective pixels and clouds (ESA, 2015). For older images (before April 2018) only Level 1C was available for download.

The Sentinel-2 Level-1C is an orthoimage product devoid of the atmospheric, terrain, and cirrus correction. This means that it is not radiometrically and geometrically corrected the Top of Atmosphere (TOA), differently from the Sentinel-2 Level-2A (ESA, 2015), which impacts in more time processing as it cannot be processed without this refinement.

4.2.3 SPECTRAL INDICES

Spectral Indices are a composition of different spectral bands and, as previously described, there are a series of spectral indices that can be better applied according to the purpose of your observation. The consensus with the area of wildfires is based on the fact that the spectral interval of the near-infrared short wave (SWIR-NIR) is considered to have a high capacity to discriminate burned areas. The reflectance values in the SWIR band increase after a fire, as it is responsible for absorbing the water present in the vegetation (Bastarrika et al., 2014).

Despite this observation, there is no consensus on which indices are the best since there is a general understanding that they can vary under different environmental conditions, types of vegetation, and different seasons (Smiraglia et al., 2020). For this research, it was decided to not determine specific indices for each type of vegetation or season, due to the short period to develop this study.

Therefore, three spectral indices were used in this research: NDVI – Normalized Difference Vegetation Index, NBR – Normalized Burned Ratio, and BAIS2 – Burned Area Index for Sentinel-2. This choice was made considering that they cover the spectral bands of Visible Infrared (VIS), Red Edge, Near Infrared (NIR), and Shortwave Infrared (SWIR) and their prevalent uses to identify burned areas.

The NDVI is one of the most common vegetation indices and is frequently used to access the stressed vegetation (Lentile et al., 2006). NDVI is a measure of the reflectivity of the plants and consequently reveals the health of the vegetation. In a healthy plant, chlorophyll strongly absorbs radiation from visible light, while the leaf cell structure strongly reflects near-infrared (NIR) light. When the vegetation becomes dehydrated, sick, affected by pests or fire, the plant absorbs more of that infrared light. Therefore, looking at how NIR varies compared to red light provides a link to plant stress (Equation 1). The index range goes from -1 to 1, where higher values represent very healthy vegetation and lower values stressed to dead vegetation.

$$\text{NDVI} = \frac{NIR - Red}{NIR + Red} \qquad\qquad \text{NDVI} = \frac{B8A - B4}{B8A + B4}$$

$$\textit{Equation 1}$$

General Formula   *Sentinel-2 Formula*

Similar to the NDVI, and largely used for the detection of burnt scars, the NBR consists of a normalized ratio between near-infrared and short-wave infrared bands (Equation 2) to differentiate the spectral behaviour of burnt and healthy vegetation (Certini, 2005).

$$\text{NBR} = \frac{NIR - SWIR}{NIR + SWIR} \qquad\qquad \text{NBR} = \frac{B12 - B8}{B12 + B8}$$

$$\textit{Equation 2}$$

General Formula   *Sentinel-2 Formula*

A strong spectral signature in the NIR band corresponds to healthier vegetation as a result of the properties of chlorophyll. When vegetation growth or regeneration occurs after a fire has occurred, the fire scar begins to be less visible and provides stronger NIR reflectance. This means that the NBR becomes less effective, as higher NIR values translate into a lower burn rate (Key & Benson, 2006). This binary detection is known as dNBR (Equation 3) and is highly reliable for estimating fire severity using pre-and post-fire images (Lentile et al., 2006). The severity classes were proposed by the United States Geological Survey (USGS) and are shown in Table 2. For a more consistent result, it is recommended to obtain images just before and after the fires.

$$\text{dNBR} = \Delta\text{NBR} = NBR_{pre\text{-}fire} - NBR_{post\text{-}fire} \qquad \textit{Equation 3}$$

Table 2: *Burn Severity Classes*

Severity Level	dNBR Range (scaled by 10^3)
Enhanced Regrowth, high (post-fire)	-500 to -251
Enhanced Regrowth, low (post-fire)	-250 to -101
Unburned	-100 to +99
Low Severity	+100 to +269
Moderated-low Severity	+270 to +439
Moderate-high Severity	+440 to +659
High Severity	+660 to +1300

The BAIS2 is the spectral index of the burnt area also known as BAI, developed especially for Sentinel-2 by Filipponi (2018) and is gradually increasing its application as seen in Filipponi (2019), Lasaponara (2006) Lasaponara (2006), Brovkina et al. (2020), Smiraglia et al. (2020) and van Dijk et al. (2021). This optimized index explores the Red-Edge spectral (703.8*nm* to 864*nm*) region presented on Sentinel-2 and the SWIR (1610.4nm to 2185.7nm) wavelengths as seen in Equation 4.

Usually spectral bands have a 0.0001 scale factor so that reflectance range between 0 and 10000 instead of ranging between 0 and 1 (Govaerts et al., 1999). When computing normalized indices (i.e. NDVI) usually the values still are in the expected range, even if the scale factor is not applied. However, many software does not apply the scale factor automatically at image opening. Since the BAIS2 formulation is not strictly a normalized index, the scale factor should be applied by the user before the index calculation to get the expected range of values (Filipponi, 2018). Thus, BAIS-2 spectral index presenting the highest values indicates burned vegetation.

$$\text{BAIS2} = \left(1 - \sqrt{\frac{B6*B7*B8A}{B4}}\right) * \left(\frac{B12 - B8A}{\sqrt{B12 + 8A}} + 1\right) \qquad \text{Equation 4}$$

Burned Area Index formula for Sentinel-2

In addition to the visual analysis of the application of these indices, the Separability Index (M) was calculated, showing the efficiency of each spectral index to detect the burnt and unburnt areas (Brovkina et al., 2020; Huang et al., 2016; Lasaponara, 2006; Smiraglia et al., 2020). In a nutshell, the Separability Index is calculated using the difference spectral index – pre- and post-fire – from each spectral index (NDVI, NBR and BAIS2) as shown:

$$M = \frac{\mu_{post} - \mu_{pre}}{(\sigma_{post} - \sigma_{pre})} \qquad \text{Equation 5}$$

Where μ_{post} and μ_{pre} are the mean values of the difference SIs for post and pre-fire, and σ_{post} and σ_{pre} are the standard deviations of the difference. If *M* higher than 1, then this spectral index is the one which better works for the detection.

4.2.4 SOFTWARE

Four main software were used for this research as described below:

- R

In order to retrieve and request the images, the free statistical software R studio was used, which is an integrated development environment with a friendly interface, facilitating the execution of the code in an exclusive console. The library used for the processes was *sen2r* which is a package specially developed to download and pre-process Sentinel-2 images.

For offline images (all year 2018 and part of 2019), *sen2r* immediately requests the data be retrieved from the online list, including archived datasets. This package also allows the user to order Sentinel-2 images in bulk, specifying a certain period. However, batching a large number of images may be impractical due to hardware requirements. A single ZIP file averages 800 MB (Level 1C) to 1.2 GB (Level 2A) of data. In addition, most of the statistical analysis were made in R.

- Command Prompt (cmd.exe)

For the Level 1C products described, pre-processing was applied using the Windows Command Prompt, which is a widely used application to automate tasks using scripts.

In this pre-processing, the *sen2cor* algorithm was used, transforming the images from 1C Level into 2A Level products. This algorithm makes corrections in orthorectification and spatial registration in the global reference system, in this case, the UTM/WGS84 projection with subpixel precision. In addition, it applies scene classification with atmospheric, terrain, and cirrus correction, converting to orthoimage L2A Bottom-Of-Atmosphere (BOA) reflectance product (ESA, 2015). The *sen2cor* is available for download on the ESA website (https://step.esa.int/main/snap-supported-plugins/sen2cor/). It was decided to make use of the Command Prompt due to its ease and quick processing than to do this operation in R.

- Erdas Imagine

It was decided for this software (Version 2020) due to its widespread use by the Geographic Information System (GIS) community and by its practicality to work with Sentinel-2 data. Erdas Imagine converts the file '.SAFE' into '.IMG' format in which can be loaded easily in other GIS software. In addition, a Script workflow in the Spatial Model Editor was used to automatize the operations for the spectral indices (Appendix I).

- ArcGIS

ArcGIS is software maintained by the Environmental Systems Research Institute (ESRI), which consists of an international supplier of GIS technology - Geographic Information System. This software is dedicated

to the creation, management, sharing, and analysis of spatial data and is widely used in the world in several science fields.

4.3 Workflow

In this subchapter, the main actions to acquire, process, and analyse the data are explained, and Figure 7 represents in a nutshell the workflow applied in this research.
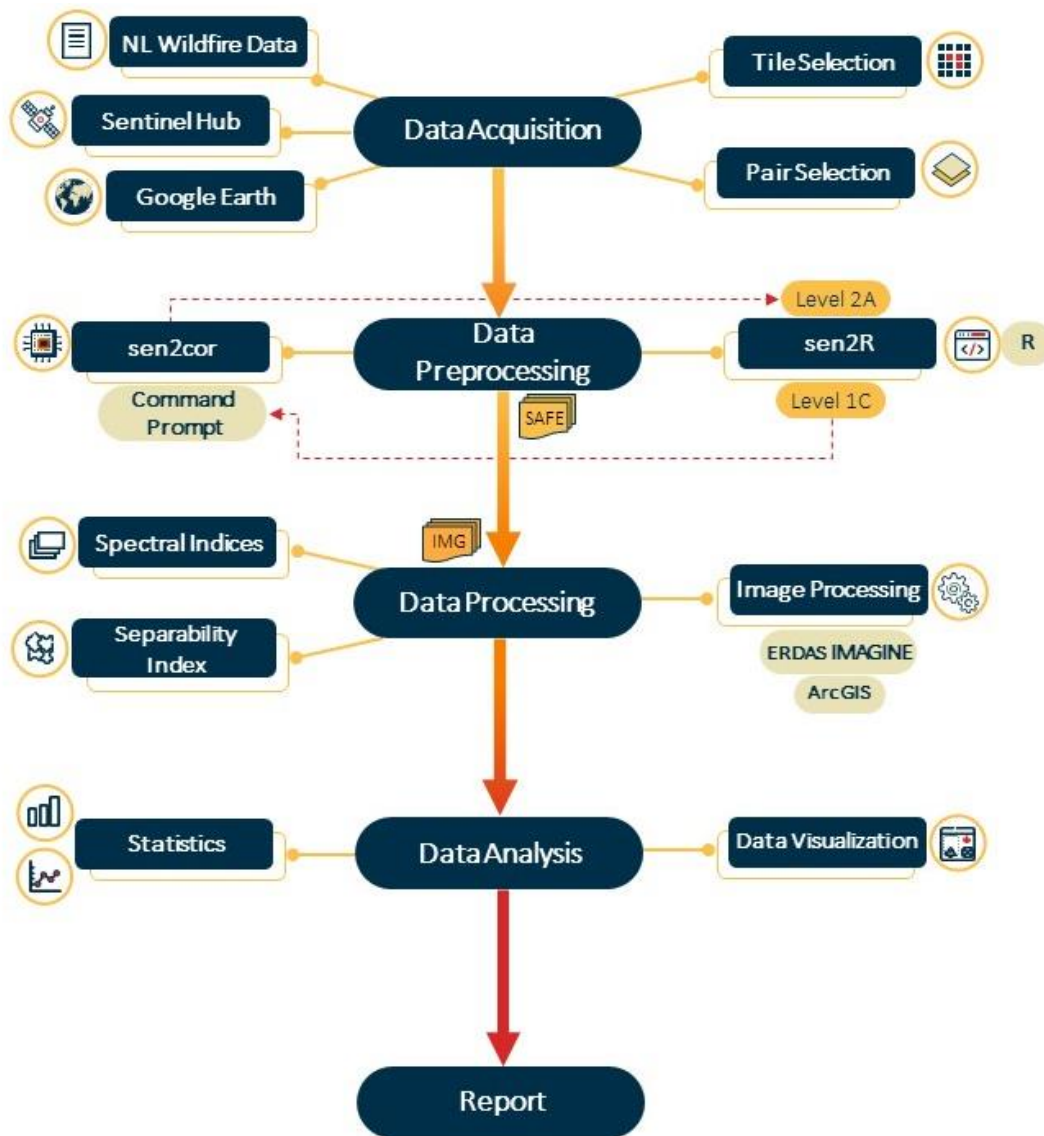
Figure 7: Workflow of the main phases.

4.3.1 DATA ACQUISITION

Based on the two fire inventory datasets with coordinates, one from Mathu (2020) and the other one developed by Herman Agricola with Dr. Jetse Stoorvogel, preference was given for fire events according to the following criteria: (i) having information about the size of the fire event - large burned areas are more likely to have a burn scar and, consequently, are more efficient for identification through spectral

indices; (ii) having information about the type of vegetation (identified as three main groups: Grassland, Heather or Forest) - small fires are more likely to be detected by remote sensing in short vegetation (grass, shrus) than in dense forests and; (iii) released information by the media - considering the low precision of the field data, this type of information could provide a good indication about more precise location of the incidents.

Moreover, it was decided to include a wildfire that occurred on April 20 in the region of Deurnese Peel. This was possibly the largest wildfire ever recorded in the country (Stoof et al., 2020) and its addition could represent valuable information in the evaluation of spectral indices. Initially 115 fire events were selected (from 2017 to 2020), however, only 88 events (Annex II) were indeed used during this study due to some constraints that will be further explained.

After the selection of these 115 potential areas, the next step was searching these fire events locations in the available images in the Copernicus Hub. Google Earth was also used for better location accuracy, guiding the selection of the appropriate tiles. Figure 8 displays the main tiles that cover the Netherlands, the main ones being UFS, UFT, UFU, UFV, UGT, UGU, and UGV.
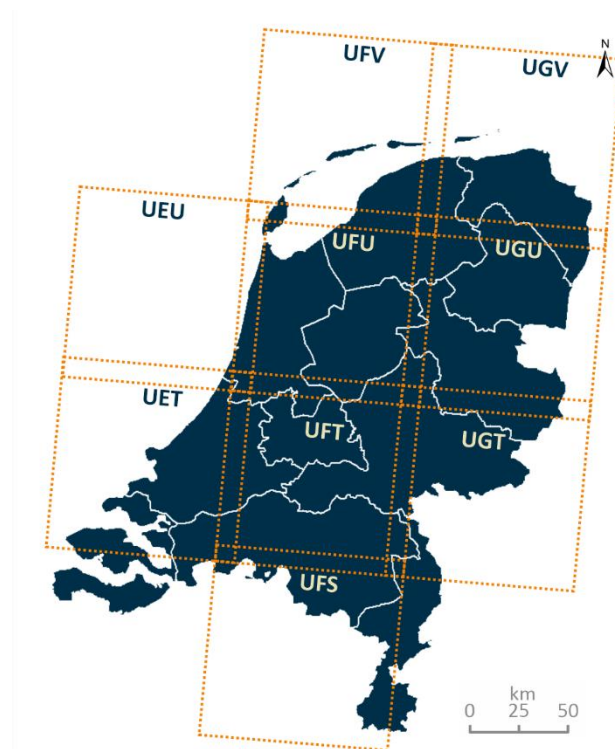
Figure 8: Main tiles over the Dutch territory.

The main difficulty at this stage was to find a proper pair of images that covers the time frame – shortly before and after – of the fire events. It should be noted that the Sentinels overpass the Netherlands in an interval that varies between 2 to 4 days. Moreover, the occurrence of clouds is a considerable limiting factor for the country.

Table 3 shows a summary of the main information over the datasets used in this research.

Table 3: Dataset information.

DATASET	2017	2018	2019	2020
N° Fire occurrences	321	949	547	-
N° events selected for the study	21	52	41	1
N° events used for the study	-	48	39	1
Satellite	Sentinel 2A and 2B	Sentinel 2A and 2B	Sentinel 2A and 2B	Sentinel 2A and 2B
Product	Level 1C	Level 1C and Level 2A	Level 2A	Level 2A
Orbit	Descending	Descending	Descending	Descending

4.3.2 DATA PRE-PROCESSING

In total 163 images were downloaded (the image inventory can be found in Annex III). Almost all images were obtained using the software R through the *sen2R* library (as described in sub-chapter *4.2.4*). For the products 1C level (images dated later than April) the algorithm *sen2cor* needed to be applied using the Command Prompt, to perform the orthorectification and to implement an atmospheric correction over water vapor, aerosol optical thickness, mask defective pixel and clouds, such other corrections, transforming into Level 2A products.

Albeit the *sen2cor* algorithm presents a cloud mask with reasonable results, it does not deliver a product 100% cloud-free. Other algorithms reduce even more the cloud cover, however, this application can cause misclassification of pixel values leading to errors in the identification of the burned patches (Fernández-Manso et al., 2016). Therefore, for this research, only *sen2cor* was used as a cloud mask option.

The final product of the pre-processing is stored in a compressed file SAFE format, containing image data in a binary data format and metadata product in XML. Each one of the products contains 800 MB to 1.2 GB of data and that is why this stage was the most time-consuming of the whole research.

4.3.3 DATA PROCESSING

The main objective in this phase was to indicate the best spectral response among the three spectral indices by visual comparison and later, by applying the Separability Index.

This stage started converting the SAFE formats to IMG formats using the software Erdas Imagine. IMG format enables easy use in other types of software and the conversion takes around 15 to 20 minutes for each product.

At this point, limitations were identified when working with images from 2017 and some from 2018. All products in 2017 showed an error message when converting SAFE to IMG format. Eventually, it was discovered that there was a problem in Erdas related to the metadata of certain Level 1C products.

An alternative to this problem was to work on these images using SNAP (Sentinel Application Platform), developed by ESA, or to download each one of the spectral bands from each image in Erdas. The time spent on both alternatives would be very large, so it was decided not to work with the images of 2017 in this research. Therefore, only the products of 2018, 2019, and the event of Deurnese Peel from 2020 were considered to continue the study.

With all products in Level 2A in IMG format, 8 fire events (from the 88 occurrences selected) with their pre and post-fire images were chosen based on the burning scar that was easily identified. In addition, the two field datasets were used to validate the result.

Taking into account these two datasets, the distance between the location of the fire event given by the field data and the real location of the burn scar identified through the true color post-fire images was measured. This process aimed to verify the biggest distance between these points and define an optimal search window (buffer) around the points, helping the visual identification of the fires in the processed satellite imagery.

Therefore, a polygon shapefile was made (buffer) highlighting each boundary of the fires selected for the model. Later, these polygons were converted to a point shapefile, taking the center of the area as a reference, and their distance to the field data was properly measured. The buffers (search-window) for the two field data were considered as the biggest distance found, to prevent any missing data as shown in Figure 9.
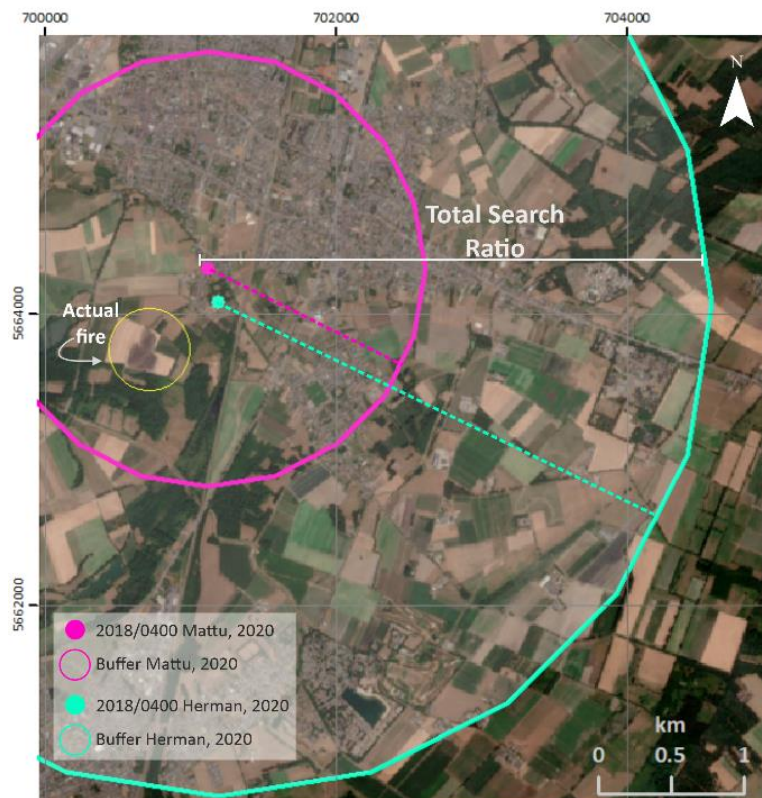
Figure 9: Example of the buffer applied for both field datasets. Fire reference: 2018_0400 (Echt - 15/07/2018). Post-fire image from 22/07/2018, shown in true colour.

For the first batch of points, the dataset from Mathu (2020) presented 1.5 km as the largest distance, while the dataset from Agricola & Stoorvogel showed a distance of 3.3 km (Table 4). Therefore, it was considered a true positive, if the burn scar was within this 3.3 km radius. It is important to note that this procedure was a visual assistance step for the identification of fire events and not as a means of verifying the accuracy of the point datasets.

Table 4: Maximum distance from the datasets for the burn scar detected.

	Fire ID	Location	City	Date	Max Distance Mathu,2020	Max Distance Agricola & Stoorvogel
2018	2018_0018	Deurnese Maria Peel	Liessel	28/02/2018	-	-
	2018_0078	Strabrechtse Heide	Heeze	21/04/2018	0.7 km	1.4 km
	2018_0104	Ginkelsche Heide	Ede	07/05/2018	0.8 km	0.6 km
	2018_0276	De Siptenpad	Tilburg	03/07/2018	0.3 km	0.05 km
	2018_0417	Kruisberg	Heemskerk	16/07/2018	1.1 km	0.7 km
	2018_0566	Sterkselseweg	Maarheeze	26/07/2018	1 km	0.15 km
2019	2019_0295	Eperweg	t Harde	18/07/2019	1.4 km	3.3 km

Subsequently, the pre and post-NDVI, NBR and BAIS2 were calculated for these 8 fire events and a visual comparison was made. In addition, the fire scar was delimited and the pre and post values of the indexes were extracted using a mask to calculate the separability index. After verifying which spectral index had the best response, the image processing was applied to the other events. And, once again, the field datasets were used to validate the possible identification of fires.

4.3.4 DATA ANALYSES

At this stage, the positively fire events detected were analyzed qualitatively through maps showing the burns scars and the dNBR. Later, some statistical analyses were also carried out to quantitatively endorse the main findings.

To answer research question 2, the correlation was calculated between the 1496 fires in the database of 2018 and 2019 with the fires detected from the satellite images with their distribution throughout the year. This process aimed to understand the frequency of occurrence during the seasons of the year, and the complete script can be found in Appendix IV.

A similar analysis was made for research question 3, where the correlation between the differences among the days of the fire and the day of the captured image to access the post-fire was made. Thus, an attempt was made to identify a pattern of days versus detection. The same was done to correlate the size of the burned area with the difference in days between fire and image, and also the correlation of the burned area with the presented severity as shown in Appendix V.

Finally, the Shapiro Wilk test was applied to understand the data distribution, and the Kruskal Wallis test was applied to verify the significance of the results.

5. RESULTS AND DISCUSSION

This section will bring up the main findings followed by the interpretations behind these results.

The methodology showed some limitations already from the analysis of the dataset. The starting point was the selection of areas with information on the type of vegetation and the area (ha) burned, but Table 5 shows that the datasets have some incomplete information, such as the total of events with the size of the burned area or information about vegetation type, which reduces the options for selecting points, as well as an overview of how small the average area burned in the Netherlands is.

Table 5: General dataset information also showing the percentage of absence data in relation to land cover and the events with no reported burned area.

	2017	2018	2019
Wildfire Occurrences	321	949	547
Reported vegetation type	60.7%	67%	43.5%
Reported burned area	44.5%	43.8%	41.6%
Average burned area (ha)	3.5	5.5	7.4
Total burned area (ha)	232	638	250

As explained in the previous chapter, 115 fire events were selected, however, due to software limitations, 21 fires chosen in 2017 were disregarded. In addition, 6 other occurrences were excluded because the images were too dark or with clouds right above the fire site. As a result, 88 fire incidents were analysed as shown in Figure 10, 48 from 2018, 39 representing 2019, and the 2020 Deurnese Peel event. With the rigorous analysis of these occurrences, it was possible to answer the research questions.

Figure 10: Location of the 88 fires used in the research.

- *Which of the applied spectral index has the best response for detecting small wildfires?*

Two approaches were used to answer this question: qualitatively with the maps visualization, and quantitatively, using the calculation of the Separability Index (M). Therefore, the three spectral indices – NDVI, NBR and BAIS - were applied for the 8 first selected areas as seen in Table 6:

Table 6: Selected points to access the capability of the spectral indices.

	Fire ID	Location	City	Land Cover	Burned area (ha)
	2018_0018	Deurnese Maria Peel	Liessel	Grassland	20
	2018_0078	Strabrechtse Heide	Heeze	Heather	10
	2018_0104	Ginkelsche Heide	Ede	Heather	7
2018	2018_0276	De Siptenpad	Tilburg	Forest	2
	2018_0417	Kruisberg	Heemskerk	Grassland	2
	2018_0566	Sterkselseweg	Maarheeze	Forest	16
2019	2019_0295	Eperweg	't Harde	Heather	15
2020	-	Deurnese Peel	Liessel	Grassland	700

The visual results can be seen in Figures 11, 12 and 13 that present the results for three events (one example for each land cover).
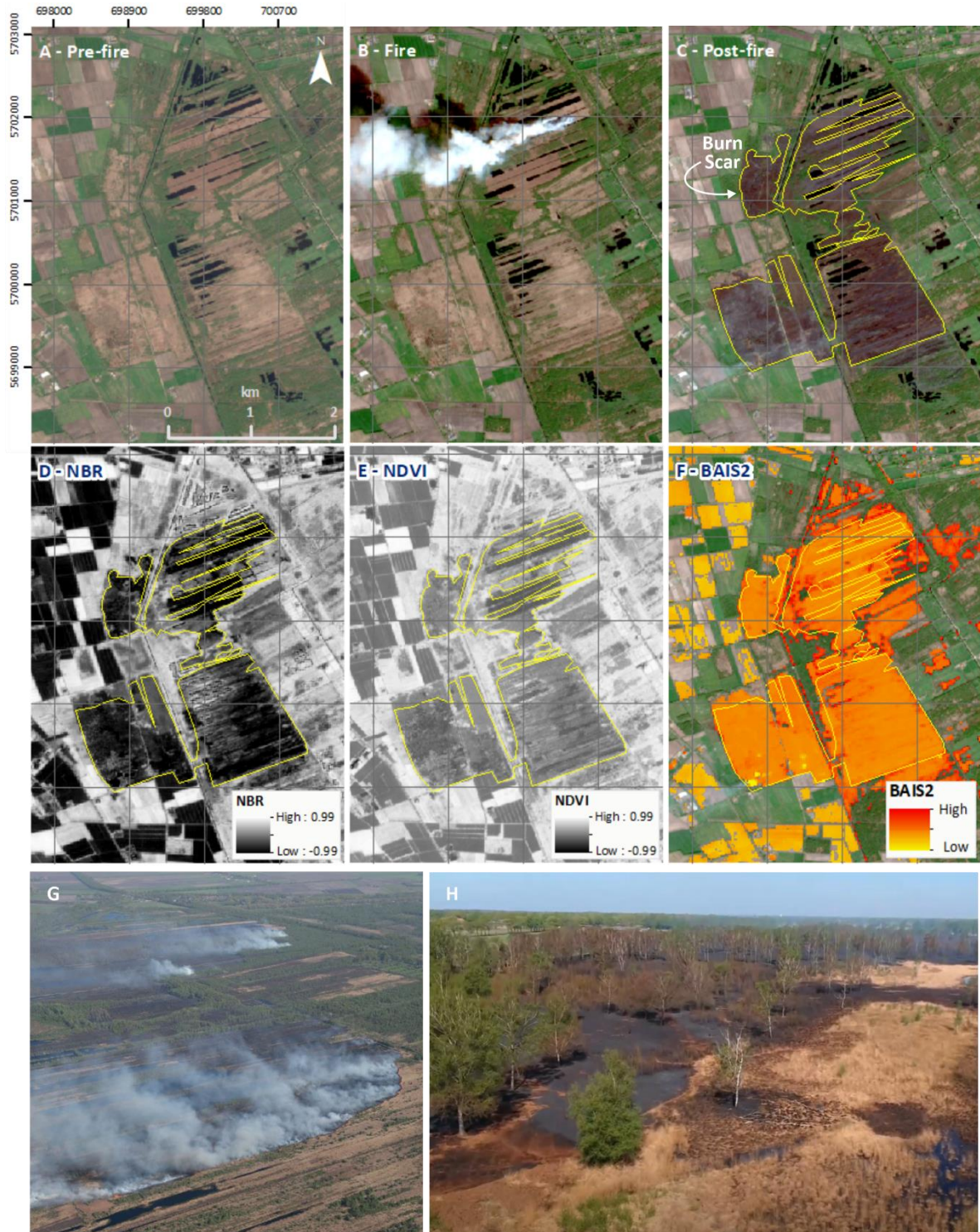
Figure 11: Deurnese Peel fire-2020 (20/04/2020) representing the grassland land cover. **(A)** Pre-fire image from 17/04, shown in true colour; **(B)** True colour image at the moment of the fire 20/04; **(C)** Post-fire image from 22/04 with evident burn scar, shown in true colour; **(D)** NBR - the darkest pixels represent the affected region; **(E)** NDVI - the darkest pixels represent the affected region; **(F)** BAIS2 – orange and reddish pixels represent the affected region; **(G)** Aerial photo during the fire. Source: http://www.wbdp.nl/onderzoeken-aan-brand-deurnesepeel?fbclid=IwAR3YHt1l_jb9yM3dc3rpeBhkKwBp2WTvEOIpOCxKKHGuZ7AC31IJZmm_Ovc and **(H)** Photo after the fire. Source: *https://www.youtube.com/watch?v=RzMwb7o-TQQ.*
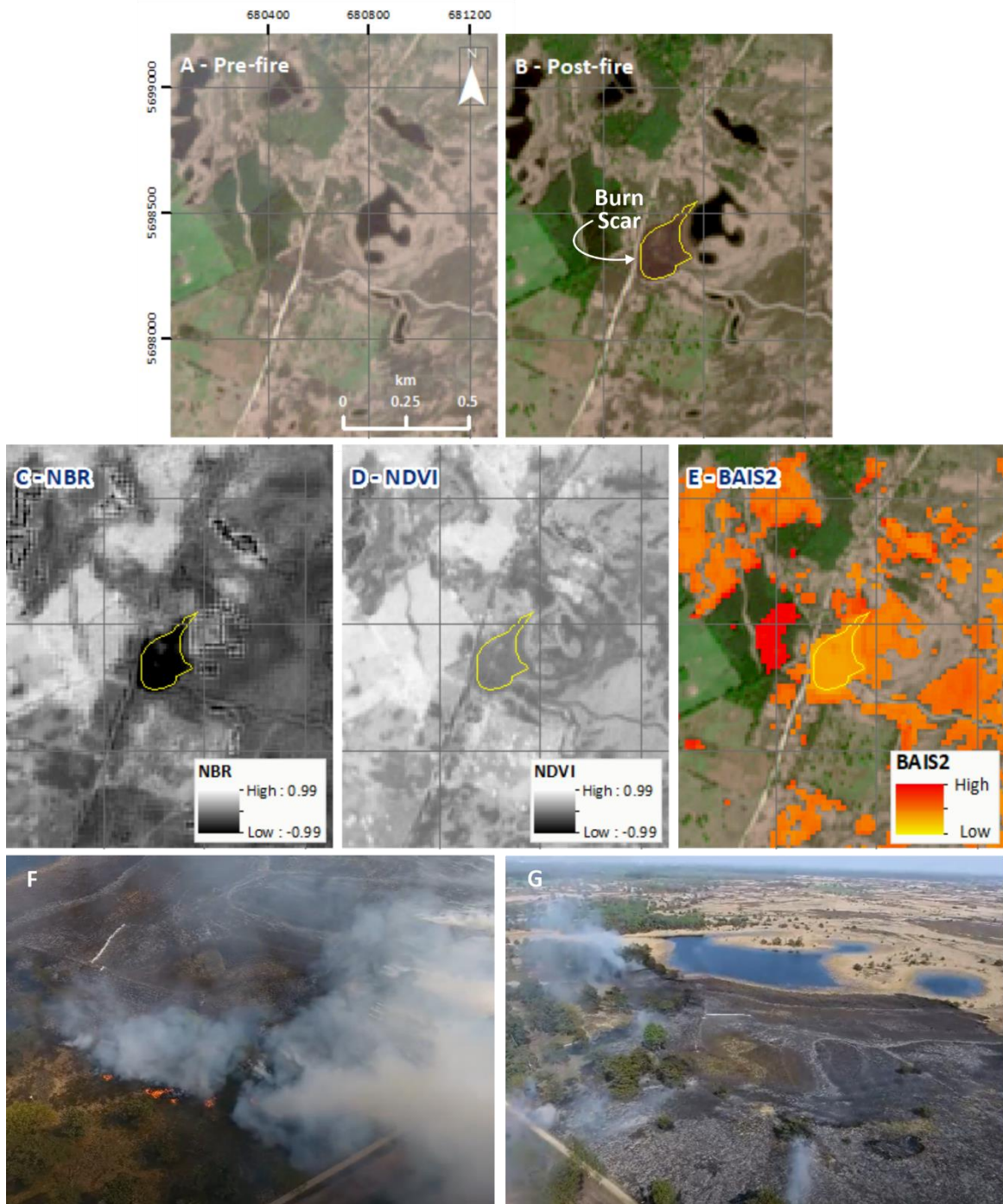
Figure 12: 2018_0078 (Heeze - 21/04/2018) representing the heather land cover. **(A)** True colour Image Pre-fire image from 18/04 in true colour; **(B)** Post-fire image from 06/05 with evident burn scar, shown in true colour; **(C)** NBR - the darkest pixels represent the affected region; **(D)** NDVI - the darkest pixels represent the affected region; **(E)** BAIS2 – orange and reddish pixels represent the affected region, with a substantial quantity of false-positives outside the burn scar limit; **(F)** and **(G)** Aerial photos during the fire. Source: *https://www.youtube.com/watch?v=Sm3USHJX8-0.*
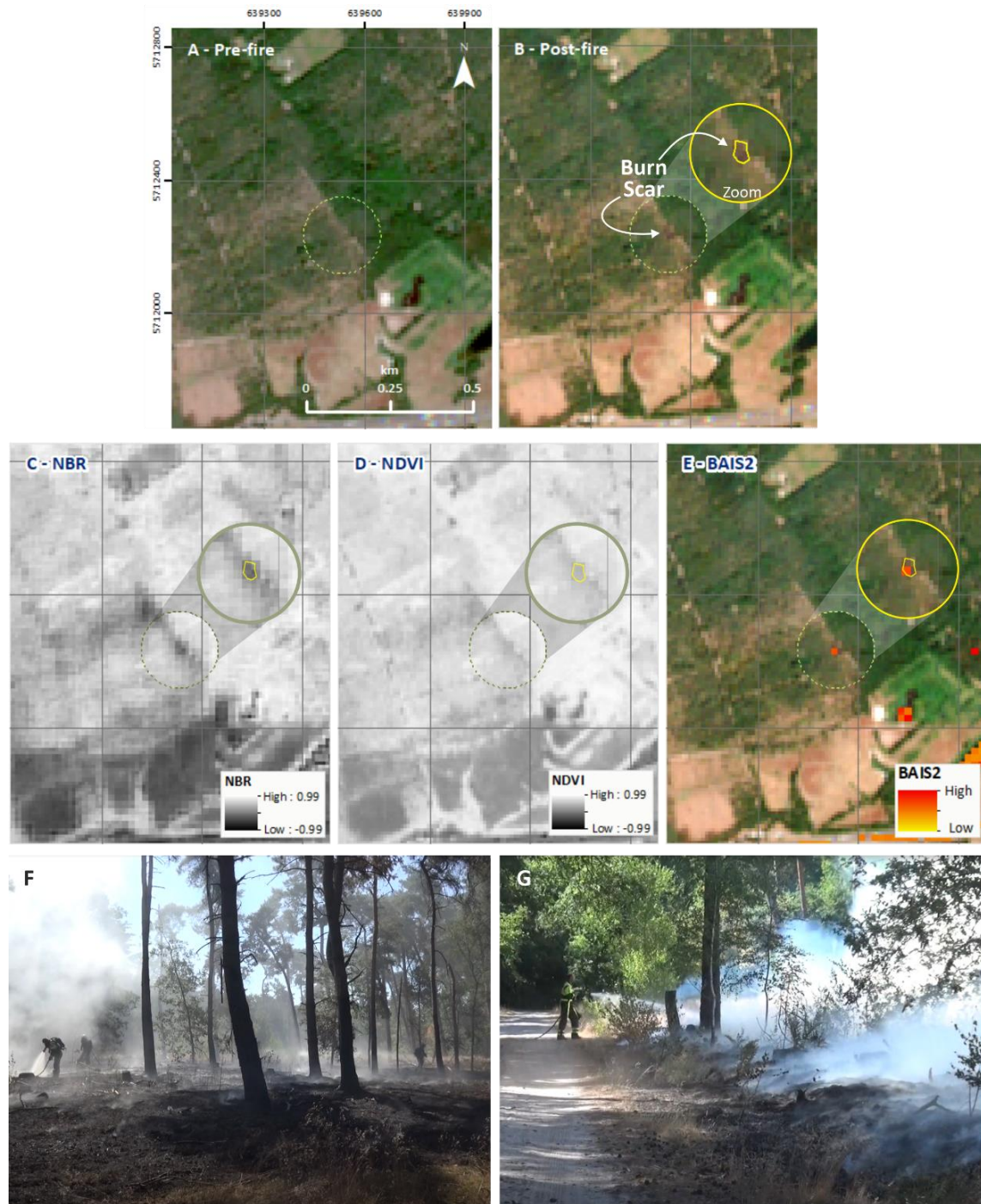
Figure 13: 2018_0276 (Tilburg - 03/07/2018) representing the forest land cover. **(A)** Pre-fire image from 02/07 in true colour; **(B)** Post-fire image from 05/07 in true colour; **(C)** NBR - the darkest pixels represent the affected region; **(D)** NDVI - the darkest pixels represent the affected region; **(E)** BAIS2 – orange and reddish pixels represent the affected region; **(F)** and **(G)** Ground photo during the fire. Source: https://www.youtube.com/watch?v=Sm3USHJX8-0.

The visual comparison analysis already highlights the difference in responses among the spectral indices. In the three locations, there is an indication that NBR shows a better discriminant capacity.

To validate these results, the Separability Index (M) was calculated for the 8 events. Figure 14 shows the comparison among the three indices proving the efficiency of the NBR over the others: the closer or greater the value to 1, the better the separability. It is important to note that the fire event 2018_0276 - Tilburg was excluded from this representation because it presented outlier values for this practice. This is perhaps because the size of the burned area - which is considerably much smaller than the other eight events analyzed - is not adequate for calculating index separability.
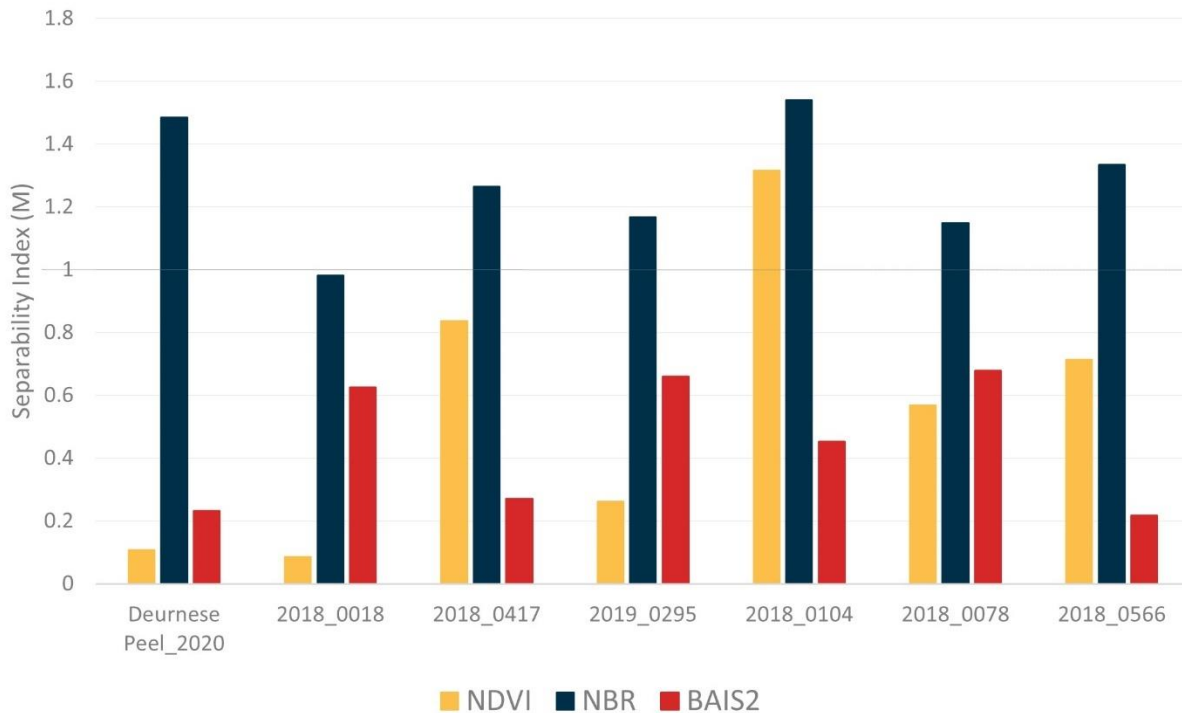
Figure 14: Separability Index (M).

The high efficiency of NBR may be the result of the different influences that each index suffers in relation to land use, as well as atmospheric influences (air humidity, albedo). As an example, NDVI has more influence on its result in wet conditions than NBR. On the other hand, BAIS2, works best when the plants are in their vegetative state (not senescent).

Some other authors also found in their researches outstanding response for NBR over other indices (Amos & Ferentinos, 2019; Filipponi, 2019; Flannigan et al., 2013; Smiraglia et al., 2020). In addition, it is important to highlight that the Difference Normalized Burned Ratio, known as dNBR is also widely used to indicate the fire severity in the landscape, which consistently proves the NBR efficiency.

Nonetheless, NBR exploits one of the biggest advantages of Sentinel-2, which is near-infrared in high spatial resolution. The relationship between the NIR and SWIR bands, in this case, reinforces the sensitive detection of changes in the Dutch landscape caused by the impact of fire. Whether in identification in grassland, heather, or forest, NBR was the most efficient among the other two indexes.

Along with the NBR, NDVI is also applied in the vast majority of wildfire studies. Typically, its application helps to identify the recovery of the fire-affected sites over a time series or even to predict regions prone to fire. As this index emphasizes the greenness of the area, it is possibly less efficient when applied to

small perimeters when compared to the NBR. This may be because the main difference between these two indices is that there is a replacement of the red band of the NDVI by the SWIR (Shortwave Infrared) in the NBR, which is much more sensitive to the change in the healthiness of the vegetation.

Conversely, BAIS2 performance was surprisingly lower than expected in this research, considering the great degree of efficiency presented in Filipponi (2018); Smiraglia et al. (2020); van Dijk et al. (2021). This index was developed to take advantage of the usability of S-2's red-edge spectral domains, which in theory would have superior results for fire detection. However, BAIS2 is a relatively new index developed by Filipponi (2018) and the possibility of using it in different types of landscapes still needs to be better studied. Nevertheless, in a later work, Filipponi (2019) stated that the NBR index performed better during the winter than BAIS2, suggesting different performances in different environments.

Specifically, in this research, BAIS2 was able to identify the burned areas, although less accurately than NBR, and it also created a series of false-positive areas. Considering that the main studies on BAIS2 were carried out mainly in the Mediterranean regions, as well as in other places where forest fires often occur on a large scale, this index produces a divergent result when applied in the Dutch landscape.

However, it is important to note that all indices have misclassification of burned pixels. Analyzing the images in detail a bias can be observed in detecting dark pixels as burnt areas. These areas generally represent a portion of bare soil, unsown fields, plowed land cover, and mainly water bodies. Thus, agricultural land is generally the biggest source of errors, representing a major challenge in avoiding this type of misclassification, especially in a country such as the Netherlands, where more than half of the country's land area is used for agriculture (OECD, 2020).

Other authors such as Filipponi (2019); Tepley et al. (2018) and van Dijk et al. (2021)), also identified agricultural terrain as one of the major sources of commission errors as it exhibits a similar spectral domain as for burned areas. In the case of the Netherlands, commission errors become even more common because of the floodplains due to the presence of ditches. The water bodies and the wet soils are characterized by low refraction values since the refractive index in this case is much lower than in dry soils. This means that in satellite images these areas are characterized by darker gray to brown tones, which implies less reflectivity.

On the other hand, rapid post-fire vegetation restoration is seen as the main cause of omission error according to some researchers (Filipponi & Manfron, 2019; Weirather et al., 2018) and which will also be seen in this study in the following pages. Typically, the severity of the fire is usually the most critical factor affecting the dynamics of nutrients in the soil. The more intense the fire, the longer the vegetation recovery time.

Nevertheless, the complexity of changes in soil chemistry after this type of event is quite high and, in general, it can be said that fire reduces the available organic matter. But despite this, fire can also increase the rate of renewal of nutrients and their distribution along with the profile of the soil and in areas where the severity was not so high. Therefore, this can lead to a quick recovery and, consequently, conceal the burn scars.

Due to the inaccuracy of the field data, no studies were carried out on commission and omission errors in this research. Thus, the detection procedure was based on the identification of a burn scar within the limit of the calculated buffers (as explained in sub-chapter 4.3.3) for both data sets and the perfect overlap given by one of the spectral indices, ignoring any other fire indications given by them.

In an attempt to increase the accuracy of the recognition of the burnt areas, the detection intervals of the three spectral were combined based on these 8 areas, as exemplified in Figure 15. It was noted, however, the wide range of intervals in the three indices, and even when observing the values for the different types of land use, the same was observed. With little expressive results, this methodology was not further carried out. Several authors Filipponi (2019); Roteta et al. (2019); Smiraglia et al. (2020), applied this technique with the adaptive intervals, however, vast statistical calculations were applied to obtain better values.
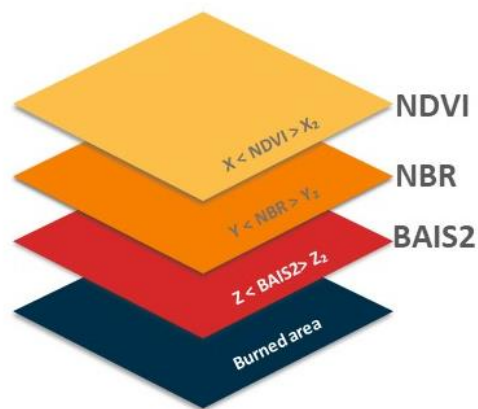
Figure 15: Combination of specific thresholds for each spectral index for better identification of burned areas.

Another alternative for better accuracy in the discrimination of wildfires is to adopt the combination of pre and post-fire images, also known as the two-phase methodology (Bastarrika et al., 2011; Flannigan et al., 2000). This procedure has recognizable efficiency for fire identification (Filipponi, 2018), considering that a single image does not emphasize changes in vegetation.

After drawing attention to all the considerations above, this research understands that the NBR (Normalized Burned Ratio) responded better among the other two indices (NDVI and BAIS2) for the identification of wildfires in the Dutch landscape. Therefore, the adoption of pre- and post-fire images will be maintained for the remainder of the research, as (i) undoubtedly presents superior results as seen in Figure 16, and (ii) it is necessary the pair of images to calculate the fire severity as previously explained in the section 4.2.3, increasing the detection efficiency.
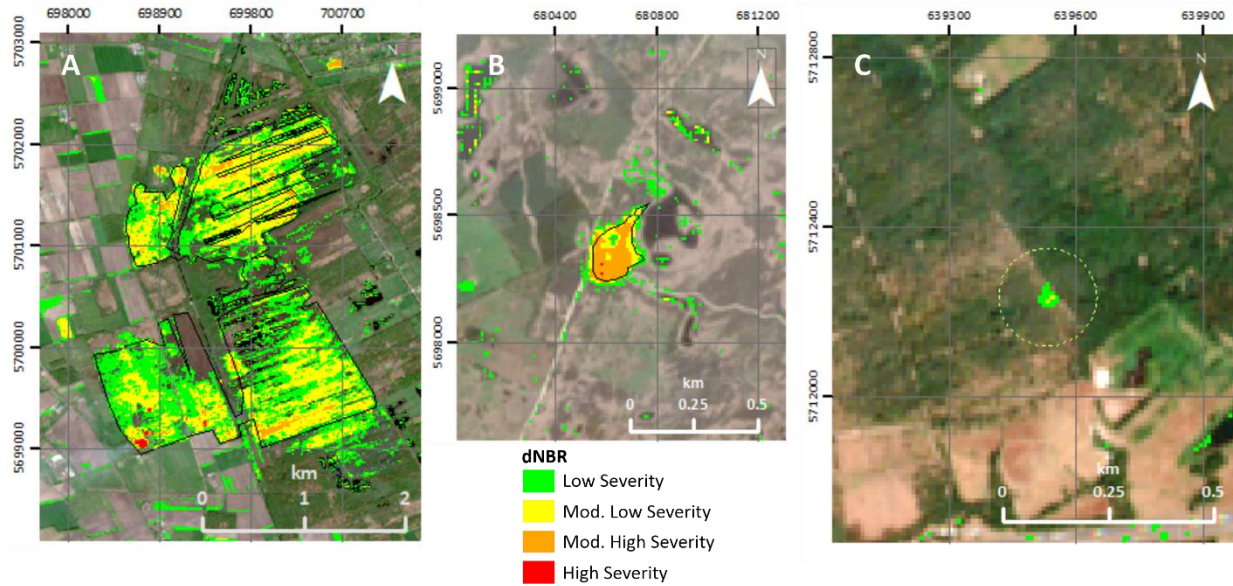
Figure 16: Same fires as studied before, but now with dNBR calculated. **(A)** Deurnesse Peel_2020 (20/04/2020); **(B)** 2018_0078 (Heeze - 21/04/2018) located in Heeze; and **(C)** 2018_0276 (Tilburg - 03/07/2018) located in Tilburg – all shown in true colour.

Thus, considering the burn scar and the dNBR calculated for the 88 selected fires, 42 were not identified, while 46 were successfully detected. Figures 17, 18, and 19 show some other wildfires identified. It is interesting to note that Figure 17 shows a good example of commission errors due to the time of harvest between the pre and post fire images. Figure 18 displays a pronounced burn scar with high burn severity, and Figure 19 exhibits one example of an image that was captured in the moment that the fire was happening.
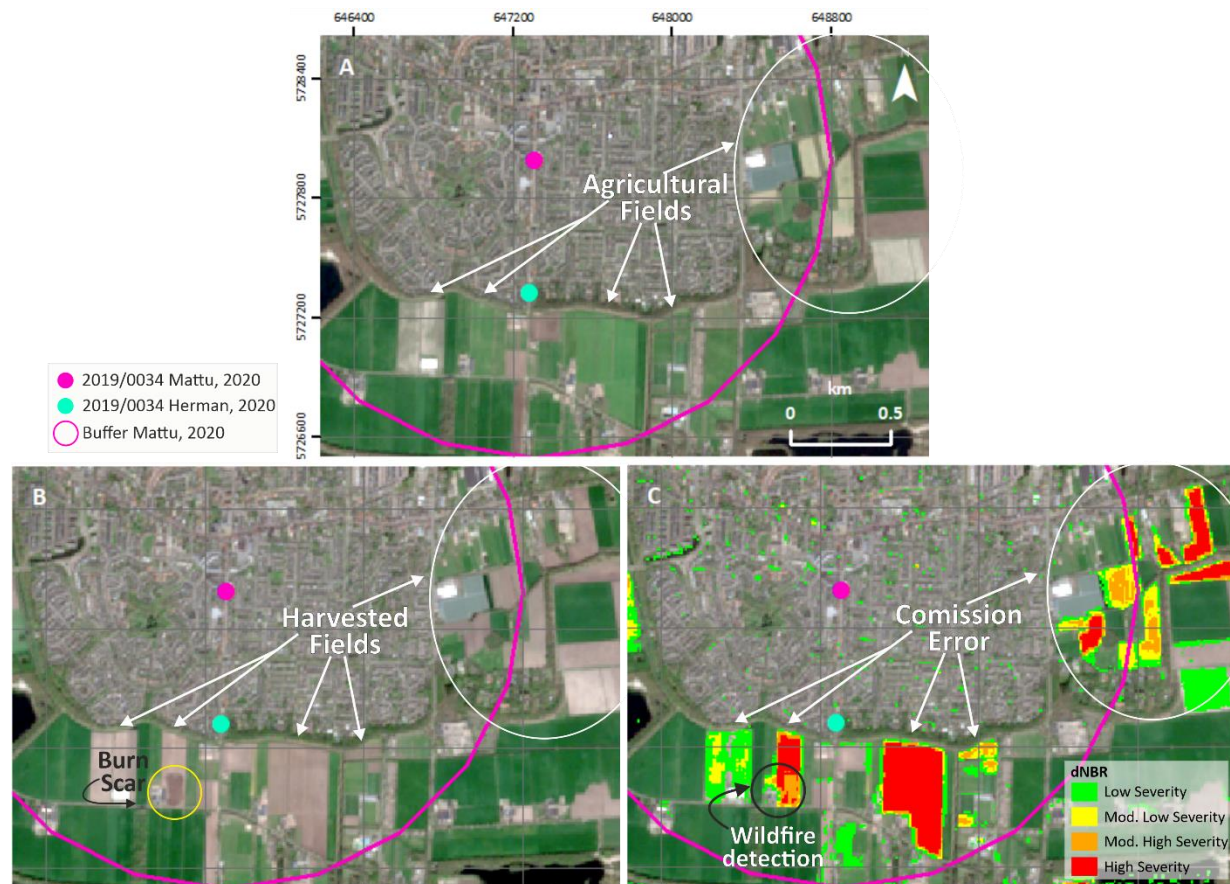
Figure 17: 2019_0034 (Drunen - 11/04/2018). **(A)** Pre-fire image from 01/04 in true colour; **(B)** Post-fire 16/04 image with evident burn scar and some harvested fields shown in true colour; **(C)** True colour image with dNBR (NBR Pre-image – NBR Post-image) displaying fire severity over the landscape with some commission errors resulted from harvested agricultural fields.
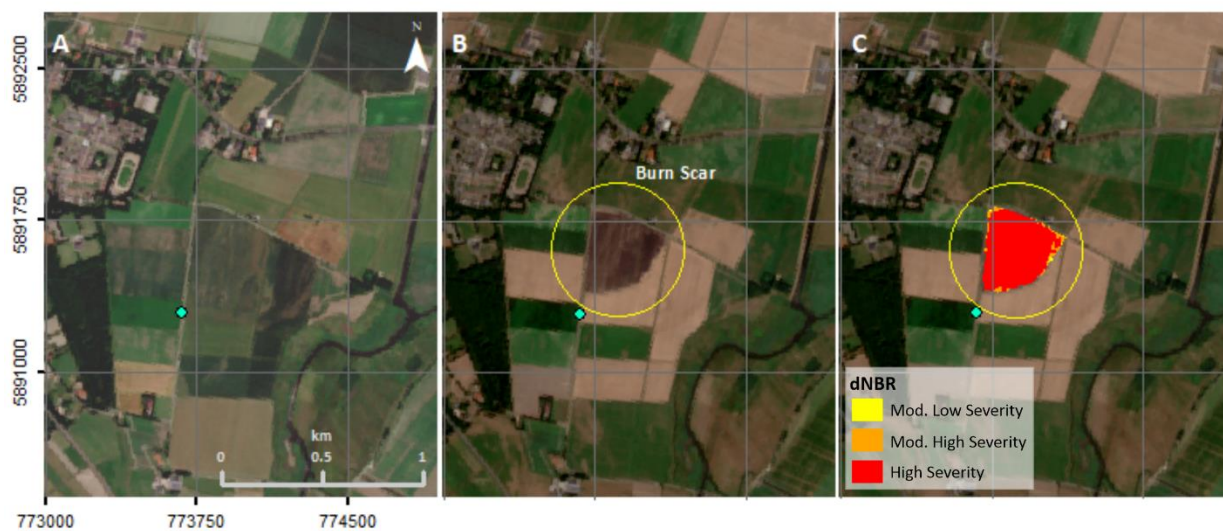
Figure 18: 2019_0337 (Blijham - 27/07/2019). **(A)** Pre-fire image from 25/07; **(B)** Post-fire image from 30/07; and **(C)** Identification of the fire through dNBR – all images in true colour.
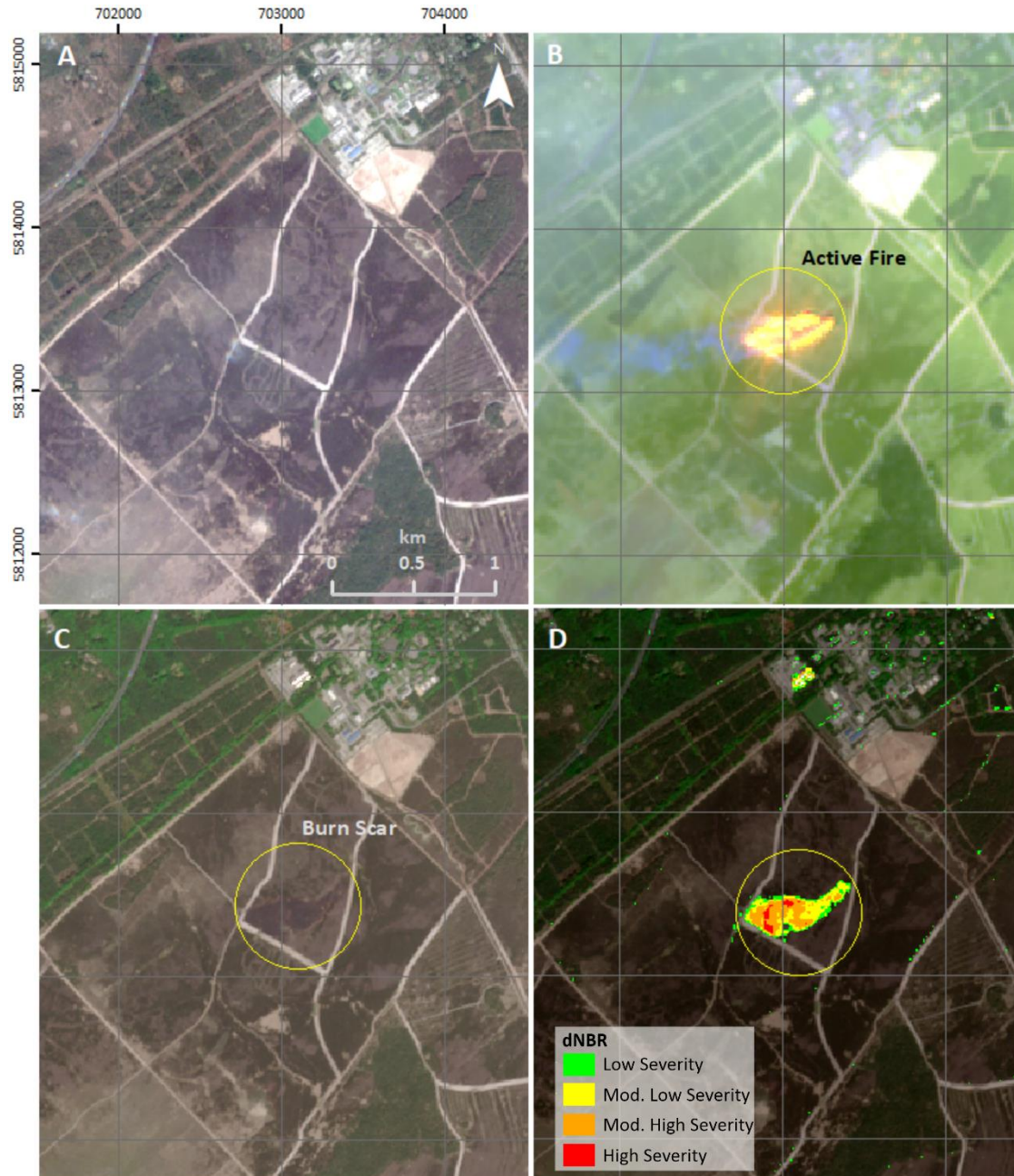
Figure 19: 2019_0533 ('t Harde- 23/04/2019). **(A)** Pre-fire image from 08/04/2019 shown in true colour; **(B)** False colour (12-11-4) image from 23/04; and **(C)** Post-fire image from 13/05 with contrast 20%; and **(D)** True colour image with calculated dNBR.

- *Will the identification of small burned areas be efficiently performed outside of the fire season?*

As previously described, clouds can be seen as an important impediment to fire recognition through satellite images, especially in the Netherlands, where one of its main characteristics is the often cloudy sky. To illustrate how challenging the analysis of these images is, Figure 20 provides a comparison of the same area on a cloudless day and on a cloudy day.
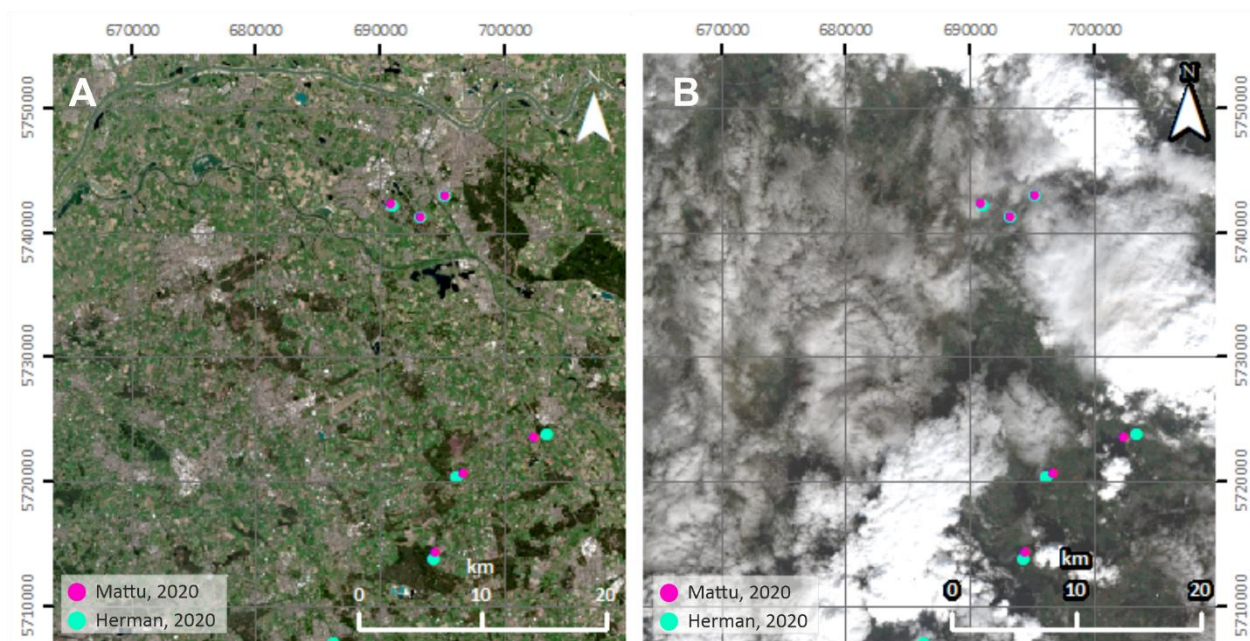
Figure 20: (A) Image Identifier: S2A_MSIL2A_20190824T105031_N0213_R051_ T31UFT_20190824T134703 from 24/08/2019; and **(B)** Image identifier: S2B_MSIL2A_20190905T104029_N0213_R008_T31UFT_20190905T135151 from 05/09/2019. Both images are displayed in true colour.

According to the historical data obtained through the website: https://www.timeanddate.com/ based on De Bilt Weather Station (De Bilt – NL), the average day temperature of the image in frame **A** was 28°C marked by sunny weather and air humidity of 37%. Captured 12 days later, the image in frame **B** was captured on a day considered cloudy, temperature of 13°C and humidity of 83%.

This example explains the idea behind this questioning. Knowing that clouds can present a great challenge for the use of satellite images, it was assumed that the detection might not be successful in months outside the fire session.

Spring is indicated as the beginning of the fire season in the Netherlands. This is because, currently, there is a decrease in relative humidity and trees are beginning to sprout. Furthermore, there are more hours of sunlight hitting the ground directly. According to Viana-Soto et al. (2017), these conditions are favourable for the ignition of grasses, shrubs, and agricultural plantations specially when you have a combination with a windy weather. In addition, the increase in the number of people enjoying the spring weather for outdoor activities such as camping and making fires, disposing of cigarettes that are still lit, or even the use of fire to clean the land, can lead to an uncontrolled fire causing damage. Thus, the premise behind this question is that in months like autumn and winter, fires will occur less frequently, and they can also spread more slowly because the climate is more humid, just as clouds would be a barrier to identifying fires outside the season.

The 1496 occurrences between 2018 and 2019 were then analysed and the percentage of events in each season was calculated as shown in Figure 21.

Figure 21: Spring (24%) with a total of 354 fires, Summer (61%) with 917 fires, Fall (11%) with 172 fires, and Winter (4%) with 57 fires.

Surprisingly, the season where the fires were most concentrated was in the Summer and not Spring. This perhaps can be explained by the peak in July and August of the year 2018 due to the severe drought that the Netherlands faced (as seen in Figure 6 in Chapter 4), which certainly influenced the numbers.

The same was done with the 46 fires identified with images from Sentinel-2 out of the 88 selected events. Notably, the result was similar to the total data (1496 fires). Spring, Summer, Fall, and Winter represent in the research sample population of 30%, 63%, 2%, and 4% respectively, as shown in Figure 22.
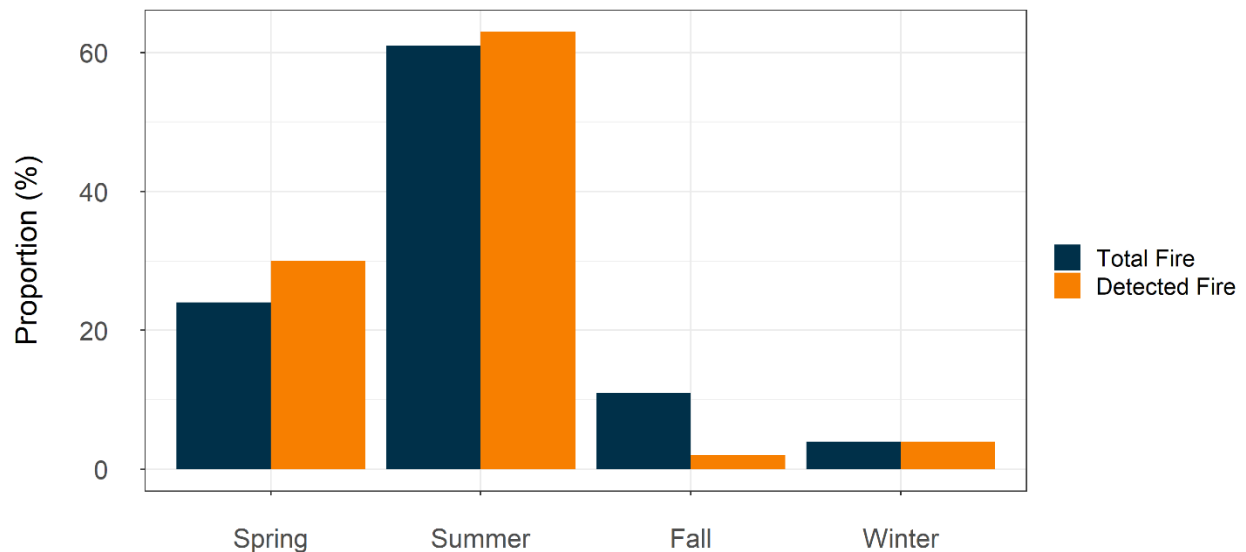
Figure 22: Proportion of the total number of fires (1496 events) in blue, distributed according to the seasons compared to the distribution of the detected fires (46 events) in orange.

This figure suggests that the identification of the fires occurred uniformly, being indifferent to the seasons. However, it is worth mentioning that the analysis was made only for 2018 and 2019, so it cannot be effectively stated that there is no trend about the period of the year. Nonetheless, in this research, can be said that the wildfires in the country can be detected even when they occur outside the fire season.

Figures 23, 24, 25 and 26 show examples of wildfires detected in the different seasons.
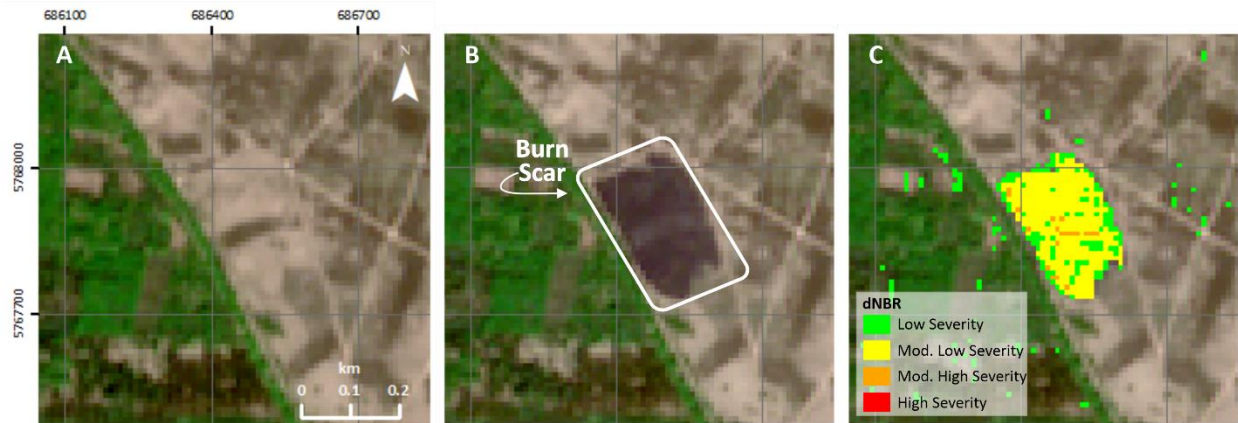
Figure 23: 2018_0104 (Ede – 07/05/2018) - Spring. **(A)** Pre-fire image from 06/05; **(B)** Post-fire image from 08/05; and **(C)** Identification of the fire through dNBR – all images in true colour.
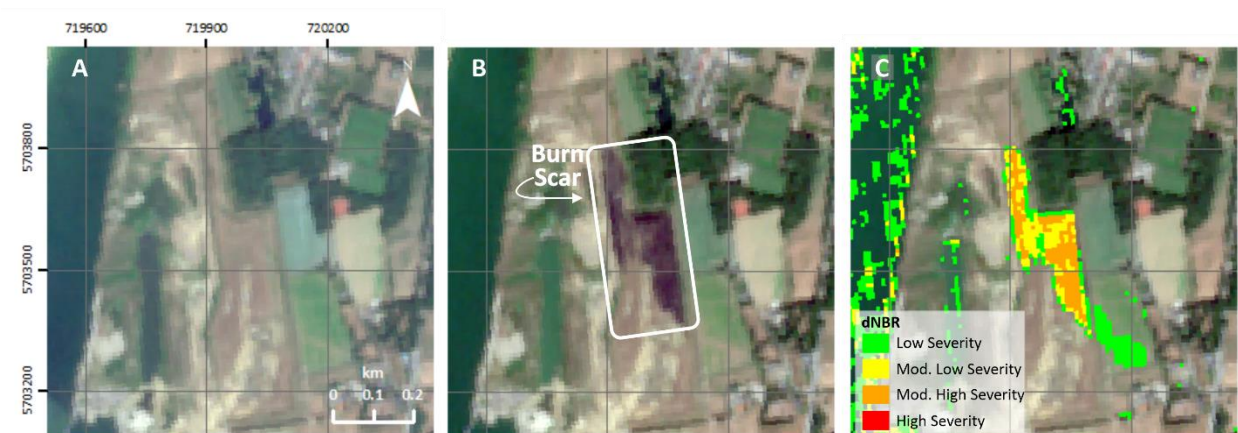
Figure 24: 2018_0642 (Lomm – 04/08/2018) - Summer. **(A)** Pre-fire image from 27/07; **(B)** Post-fire image from 06/08; and **(C)** Identification of the fire through dNBR – all images in true colour.

Figure 25: 2019_0642 (Budel – 15/09/2019) - Fall. **(A)** Pre-fire image from 31/08; **(B)** Post-fire image from 20/09; and **(C)** Identification of the fire through dNBR – all images in true colour.

33
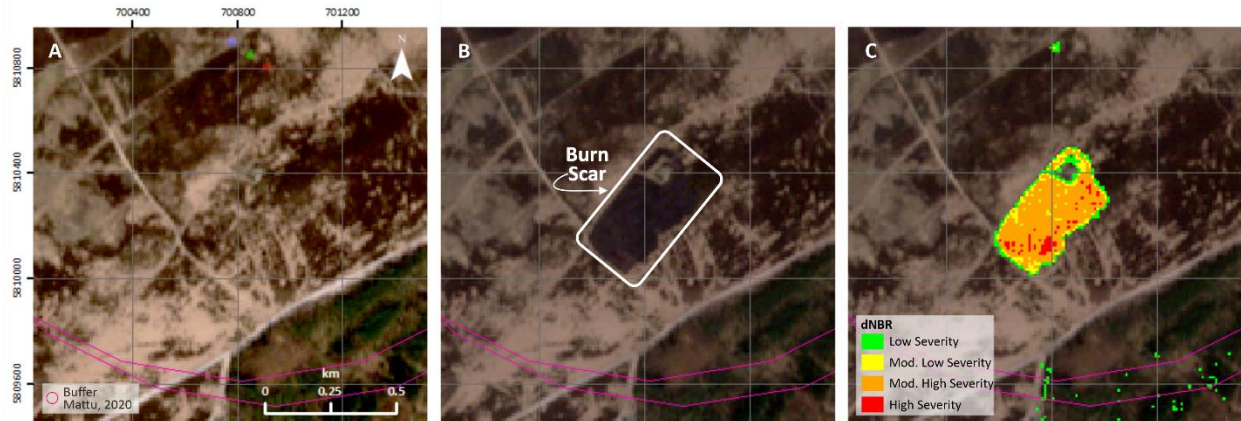
Figure 26: 2018_0020 ('t Harde – 28/02/2018) - Winter. **(A)** Pre-fire image from 25/02; **(B)** Post-fire image from 02/03; and **(C)** Identification of the fire through dNBR – all images in true colour.

Both Figures 23 and 24 (Spring and Summer respectively) show events with evident burn scar and moderate severity, whereas Figure 25 (Fall) present a very small fire with low severity. Figure 26 representing a fire event from winter, reveal a significant burn scar with a considerable severity.

- *How long after a fire has occurred can it still be detected?*
  - *Does this depend on the size and/or severity of the wildfire?*

Possibly this is an important issue for understanding the success of wildfire detection in the Netherlands using images from Sentinel-2.

As mentioned before, one of the main limitations in this research was to find a proper pair of images shortly before and after the fire. This is because the country is known for its cloudy weather that may make it impossible to acquire fair images. Taking this into account, it was calculated the difference in days of the fire event with the date of the post-fire image as shown in Figure 27.
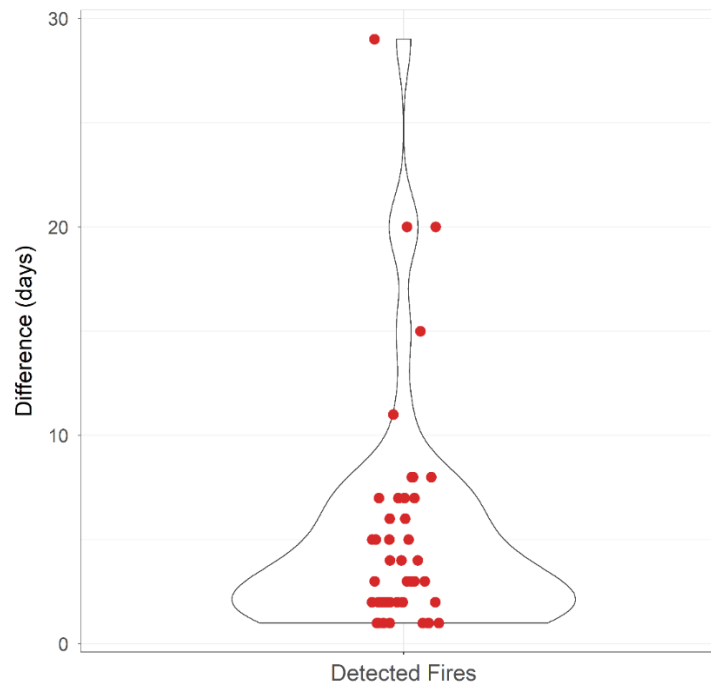
Figure 27: Difference in days from the date of the fire occurrence and the post-fire image.

Of the 46 fires identified, 41 have post-images up to a maximum of 10 days after the occurrence of the event, with an average of 5.17 days and a standard deviation of 5.71. The maximum number of identification days was in fire 2019_0271 with a difference of 29 days between the event and the image, followed by two more sites (2019_0156 and 2019_0533) with a difference of 20 days.

The Shapiro-Wilk result revealed that the data do not have a normal distribution and by the Kruskal-Wallis test, the p-value is equal to 0.03. This means that the gap between the fire date and the post-fire image date is highly significant for detection. Thus, the time between the fire and acquisition of the satellite image influences identification: the shorter the date differences, the greater the identification.

The interval of days between the fire with the posterior image may also be enough for the vegetation recovery – even if partial - resulting in the disappearance of the burn scar. As said before, the lack of studies about the Dutch wildfires can limit certain conclusions about the post-fire vegetation recovery.

Authors such as Stoof et al. (2013), Tepley et al. (2018) describe that the recovery of vegetation depends on factors such as topography, type of vegetation, type of soil, climatic conditions, severity, and frequency of fires in the region. In addition, most studies on vegetation recovery are carried out in large burned areas. Due to their size, these areas have a more complex ecosystem, which may lead to a slower recovery rate.

Another important point indicated by Lacouture et al. (2020) is that the spread of seeds - through birds and/or winds - from healthy areas nearby for the affected areas, helps immensely in vegetation recovery. Of the 8 areas they studied around different regions of the USA, Lacouture et al. (2020) were able to conclude that grass and flowering plants have a faster recovery when compared to other types of vegetation, suggesting a great resilience of these species.

Therefore in this context, it can be assumed that overall the Dutch areas affected by fire, may have a capacity for rapid regeneration. It is worth pointing out once again, that this is a roughly interpretation since several variants influence the recovery of vegetation cover that is not being discussed here. Figure 28 exemplifies a case of quick vegetation recovery, 12 days after the fire event in an agricultural field.

Figure 28: 2019_0303 (Kessel – 23/07/2019). **(A)** Pre-fire image from 27/06; **(B)** Post-fire image from 25/07 – 2 days after the fire – with clear burn scar; and **(C)** Post-fire image 2 from 04/08 – 12 days after the fire – with no evidence of burn scar.

- *How long after a fire has occurred can it still be detected?*
  - *Does this depend on the size and/or severity of the wildfire?*

It is interesting to note certain singularities when analysing the total affected area of the 1496 events. According to the data from Agricola & Stoorvogel, of all incidents recorded between 2018 and 2019, only 476 had information about the size of the burned areas. This represents only 31.8% of the entire dataset and the average area of these events is approximately 1.4 hectares.

Considering the dataset inaccuracy, it was decided to calculate the burned area of these 46 events by using the Sentinel-2 images based on the burn scar and the dNBR. Remarkably, the average of the detected areas was around 14.1 ha, showing that the affected sites are almost 65% on average larger than those recorded in the dataset. Therefore, with the area's sizes derived from the images, a relationship was made with the difference in days of the fire, with the post-fire image as shown in Figure 29. It is important to note that the Deurnese Peel fire that occurred in 2020, was excluded from this analysis as it represents a singular event in the country where it burned more than 700 ha of land.

Figure 29: Distribution of the burned area (ha) over the difference in days of the fire occurrence and the available post-fire image.

The statistical analysis showed a non-Gaussian distribution and a p-value equal to 0.3. This means that the size of the area has little influence on the fires identified here. The idea behind this research question was that the bigger the area, the longer the vegetation recovery time as this is usually found in most researches. However, as already discussed in this work, almost all studies in the academia are carried out in burned areas above 100 ha, which indicates complex ecosystems and sites with a known fire history.

But above that, this figure indicates a concentration of more than half of the fires with a maximum of 20 ha that were identified until the 10th day after the event. But how to explain an area of just 6 ha having been identified 29 days after the fire?

Randerson et al. (2012) in an attempt to quantify the total biomass burned from small fires, revealed that severity is one of the main elements for the identification of these events. This research also points out that part of the false positives given through the dNBR are in most cases labeled as low severity, and in the same matter, true positives present a severity above the low severity.

Considering this, the severity of the event 2019_0271 that burned 6 ha and was identified 29 days after the fire, was compared with three other locations (2018_0066, 2018_0263 and 2018_0417) with similar area size and which were identified in images obtained 3 days after the date of the event. The difference in severity can be seen in Figures 30, 31,32 and 33.

Figure 30: Fire 2019_0271 (Voerendaal – 06/07/2019). **(A)** Pre-fire image from 27/06 in true colour; **(B)** Post-fire image from 04/08 (29 days after the fire event) with clear burn scar, shown in true colour; and **(C)** True colour image with dNBR calculated 29 days after the fire.

Figure 31: 2018_0066 (Tubbergen - 18/04/2018). **(A)** Pre-fire image from 06/04 in true colour; **(B)** Post-fire image from 21/04 (3 days after the fire event) with clear burn scar, shown in true colour; and **(C)** True colour image with dNBR calculated 3 days after the fire.
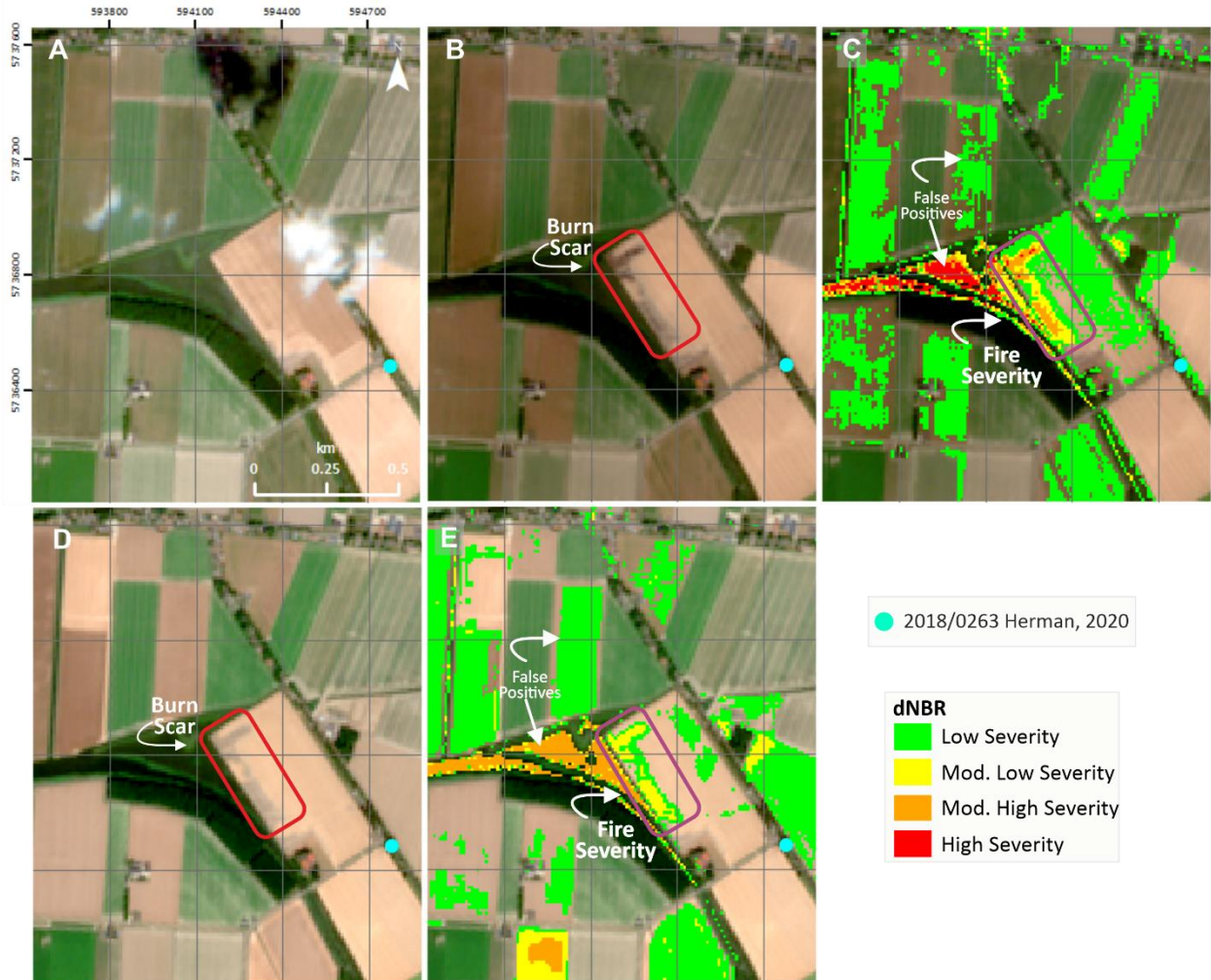
Figure 32: 2018_0263 (Zuid-Beijerland - 02/07/2018). **(A)** Pre-fire image from 30/06 in true colour; **(B)** Post-fire image from 05/07 with clear burn scar, shown in true colour; and **(C)** True colour image with dNBR calculated 3 days after the fire. **(D)** Post-fire image from 15/07 with lighter burn scar, shown in true colour; and **(E)** True colour image with dNBR calculated 13 days after the fire showing lower severity.
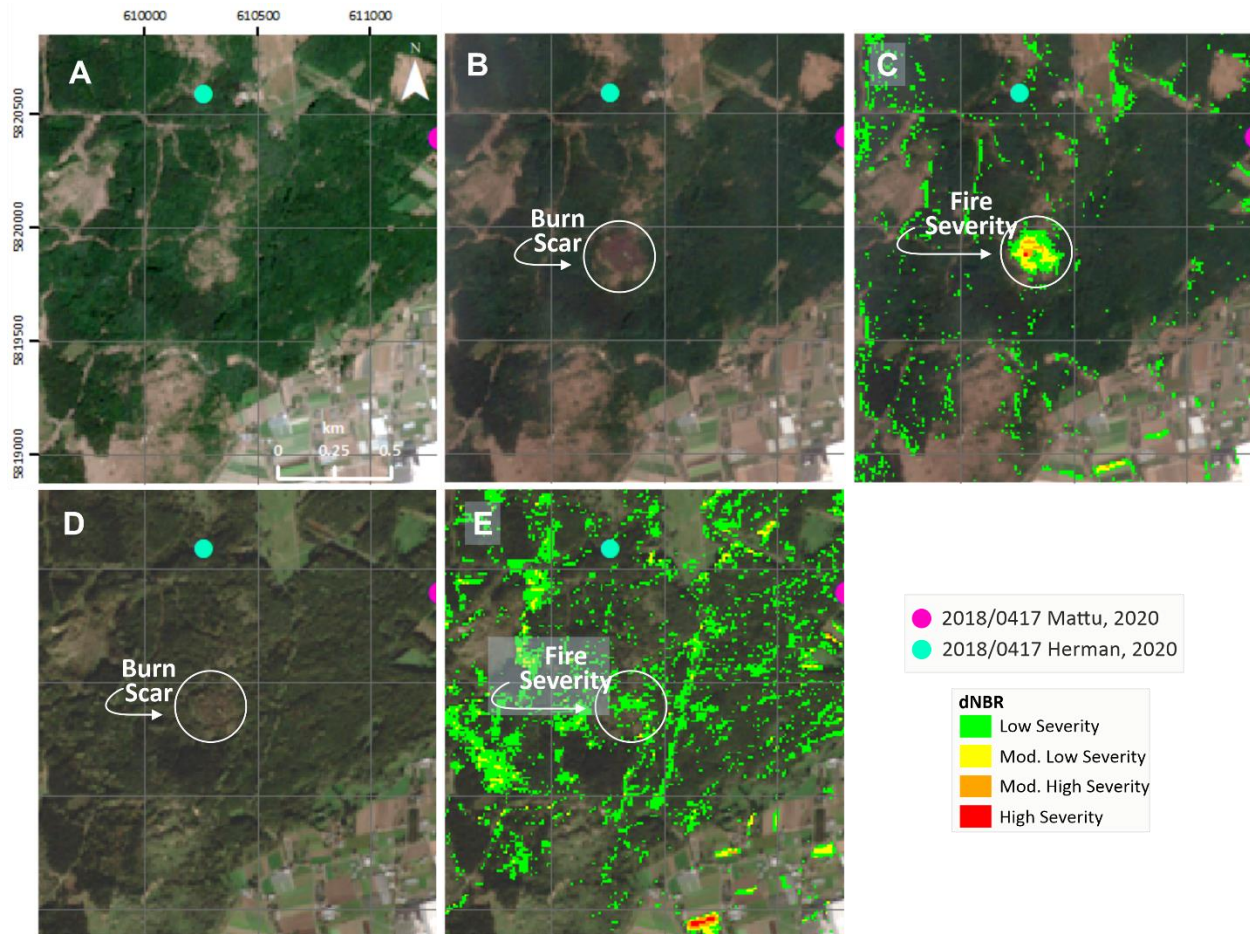
Figure 33: 2018_0417 (Heemskerk - 16/07/2018). **(A)** Pre-fire image from 15/07 in true colour; **(B)** Post-fire image from 20/07 with clear burn scar, shown in true colour; and **(C)** True colour image with dNBR calculated 5 days after the fire. **(D)** Post-fire image from 14/08 with no evident burn scar, shown in true colour; and **(E)** True colour image with dNBR calculated 29 days after the fire showing low severity, or a commission error.

The images above represent how severity plays an important role in fire detection. As shown in Figure 30, the fire 2019_0271 was recognized after 29 days and was the one with the greatest severity when compared to other fires of similar area size and lowest severity, even being identified immediately after the fire.

Figure 31 shows the fire 2018_0066 identified after 3 days of the incident, being possible to observe the low severity given by the dNBR. Unfortunately, there were not enough good images of this region to verify the event after a few days.

Figure 32, represented by 2018_0263, presents a moderate severity after 3 days of the event. The interesting thing to note is that the dNBR calculated 13 days after the fire, displayed on frame D, there is a smoother burn scar and much lower severity (frame E). This exemplifies how the area's recovery stage can influence detection. Another similar example is shown by Figure 33, fire 2018_0417, where 28 days after the fire it is no longer possible to identify a clear burn scar and, has limited detection by the dNBR calculation.

The severity was therefore analyzed for the 46 wildfires, proving that the majority had moderate high to high severity, which indicates the considerable role of the severity for the small wildfires detection (Figure 34). The data presents itself as not normally distributed and the p-value equals to 0.04 meaning a large significance of the severity.
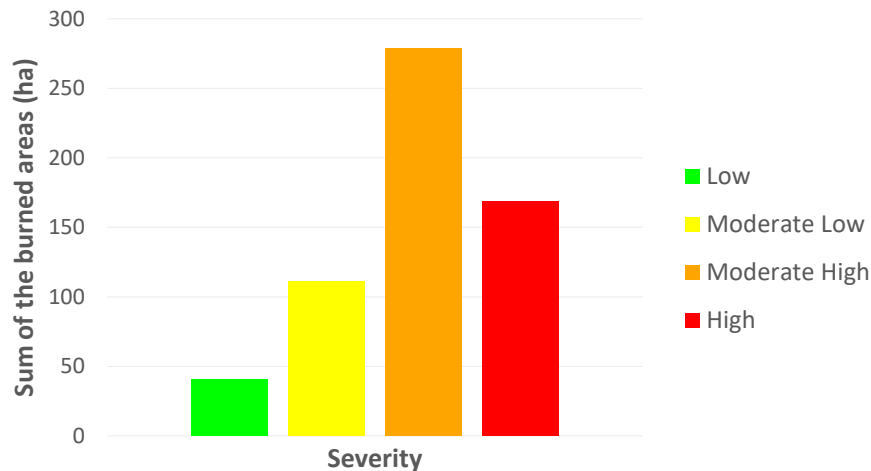
Figure 34: Severity present in the studied fires. Low Severity - 7%, Moderate to low severity – 17%, Moderate to high severity – 47%, and High severity – 29%.

This proves once again that the severity is more significant for the recognition of fires than the total area burned. And in addition, obtaining an image right after the event is highly recommended for the success of the identification.

As a result, the main research question can be answered:

Can small burned areas be identified using Sentinel-2 data?

Yes, it is possible to identify small fires in the Netherlands using Sentinel-2 images, however, with certain limitations. Although intuitive, this research showed how much clouds are an important factor in this matter. The lack of good images, especially after the fire, was a very strong limiter for the study. However, of the 88 events selected for the analysis, 46 fires (52% of the sample) were effectively recognized through the burned scars with the calculation of the dNBR.

However, it is safe to say that the biggest constraint was the imprecise field data. The inaccuracy in the two datasets (Mathu, 2020; and Agricola & Stoorvogel) can be seen already in the difference in coordinates that the same fire event can have. This resulted in a greater difficulty in identifying the burnt areas and using this field data as validation dataset. In addition, uncertain or missing information, such as the size of the burnt area, land cover, and the cause of the fire, significantly restrict possible interpretations of the fire's behaviour.

The promising calculation of the dNBR sometimes resulted in confusing false positives, reflecting the great fragmentation of the Dutch landscape. Perhaps in future research, this can be minimized with the use of information on land cover and perform a filter for agricultural areas, bare soils, and water bodies, hence avoiding some commission errors.

Furthermore, this research has come to the understanding that in addition to the inaccurate field data, the difficulty in analysing burnt areas in the Netherlands is partly due to the great heterogeneity of the landscape, as seen in Figure 35.
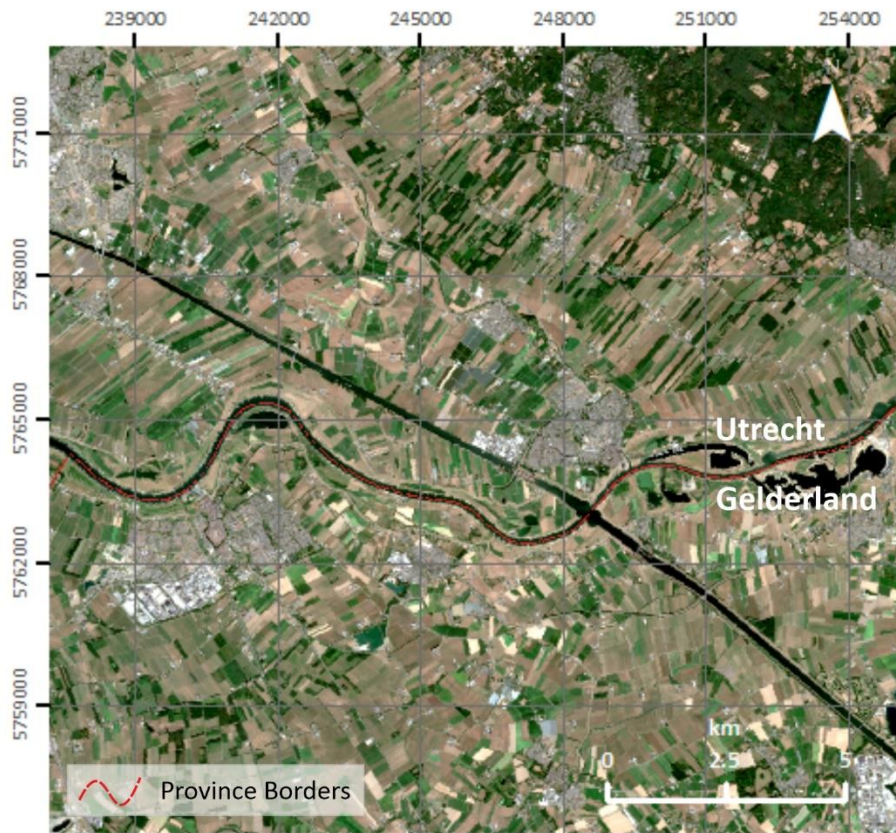
Figure 35: Area between Utrecht and Gelderland's Provinces as an example of the fragmented Dutch landscape on 06 August 2018. Image: S2A_MSIL2A_20180806T104021_N0208_R008_T31UFT_20180806T142805

This is a simple demonstration that even though the Netherlands is not as seriously affected as other countries, the study of fires here is also a challenging task, considering this multiplicity in its landscape, which is quite different from the study areas of the studies used as references. This heterogeneity may be one of the reasons for the occurrence of small fires; this fragmented landscape results in small patches of different land covers, limiting the spread of the fire, because they do not offer the necessary and/or a similar amount of fuel for the continuity of the fire.

In a final analysis considering the results obtained and some limitations found, the identification of small burnt areas can be suitably identified using the images from the Sentinel-2 satellite.

6. RECOMMENDATIONS

This was one of the first researches using remote sensing to assess this environmental risk in the Netherlands, and in general, it was satisfactory in its purpose. However, much still can and must be done to gain a better understanding of Dutch fires. In the case of Sentinel-2, this research points out an

enormous potential in the use of the MSI sensor and in acquisitions with 10 to 20 meters of spectral resolution. Spectral indexes such as Mid-Infrared Burned Index (MIRBI), Soil-Adjusted Vegetation Index (SAVI), and the assessment of the Red-Edge Bands (Bands 5, 6, and 7) in the NDVI calculus, as well as the application of bands 11 and 12 for the NBR as studied by Amos and Ferentinos (2019), can be explored in future research.

Another alternative that can be efficient is the use of another methods of remote sensing, such as Sentinel-1. Differently from Sentinel-2, Sentinel-1 is an active sensor provided with SAR (Synthetic Aperture Radar) technology that provides for the user, high spatial resolution through advanced techniques. In addition, because Sentinel-1 is equipped with RADAR (Radio Detection and Ranging), cloud images are no longer an issue. Furthermore, satellites from other space agencies could be further explored, such as JAXA and some private companies that sometimes provide open data from their products. These satellites may perhaps provide images captured on other dates that may not have as much cloud cover.

In addition, some recent studies (Roteta et al., 2019; Smiraglia et al., 2020) have used the development of algorithms that combine different spectral indices and specific detection intervals to identify the burned areas more accurately.

However, none of the above recommendations will be truly effective if the data in the field is not obtained more completely and accurately. It is worth remembering that the field data used were acquired in a particular partnership between Netherlands Fire Service and the Institute for Physical Safety and Wageningen University & Research. Thus, it is strongly encouraged that the services responsible for this type of data collection in the Dutch territory become more present and efficient, otherwise, little or limited knowledge will be gained about wildfires in the Netherlands.

7. CONCLUSIONS

Accurate data and information on the occurrence of wildfires are essential to assist the management of this environmental risk. This goes for defining planning strategies, interpreting cause and effect relationships, working on a possible restoration of vegetation, and mainly, avoiding environmental losses and damage to living beings.

This research sought to advance on the application of high-resolution satellite images (10 to 60 meters of spatial resolution) to materialize as an alternative to analyse this problem in the country. Limitations such as data inaccuracy and presence of clouds were some of the factors that somewhat limited the study.

Nevertheless, the application of the two-phase methodology for the NBR, known as dNBR, proved to be very efficient together with the verification of the burned scars for the identification of fires. In addition, this method shows the fire severity, which is one of the main factors for the recognition of fire events, being even more decisive than the size of the burned area. Although there are some restrictions, the analysis of the Sentinel-2 images proves that its application can and should be harnessed for the study of Dutch fires.

8. REFERENCES

Amos, C., & Ferentinos, K. (2019). Determining the use of Sentinel-2A MSI for wildfire burning & severity detection. *International Journal of Remote Sensing, 40*, 905-930. doi:10.1080/01431161.2018.1519284

Artés, T., Oom, D., de Rigo, D., Durrant, T. H., Maianti, P., Libertà, G., & San-Miguel-Ayanz, J. (2019). A global wildfire dataset for the analysis of fire regimes and fire behaviour. *Scientific Data, 6*(1), 296. doi:10.1038/s41597-019-0312-2

Bastarrika, A., Alvarado, M., Artano, K., Martinez, M., Mesanza-Moraza, A., Leyre, T., . . . Chuvieco, E. (2014). BAMS: A Tool for Supervised Burned Area Mapping Using Landsat Data. *Remote Sensing, 6*, 12360-12380. doi:10.3390/rs61212360

Bastarrika, A., Chuvieco, E., & Martín, M. P. (2011). Mapping burned areas from Landsat TM/ETM+ data with a two-phase algorithm: Balancing omission and commission errors. *Remote Sensing of Environment, 115*(4), 1003-1012.

Belenguer-Plomer, M. A., Tanase, M. A., Fernandez-Carrillo, A., & Chuvieco, E. (2019). Burned area detection and mapping using Sentinel-1 backscatter coefficient and thermal anomalies. *Remote Sensing of Environment, 233*, 111345. doi:https://doi.org/10.1016/j.rse.2019.111345

Boschetti, L., Roy, D., & Justice, C. (2009). International global burned area satellite product validation protocol. *Part I-Production and standardization of validation reference data*, 1-11.

Bowman, D., Balch, J., Artaxo, P., Bond, W., Carlson, J., Cochrane, M., . . . Pyne, S. (2009). Fire in the Earth System. *Science (New York, N.Y.), 324*, 481-484. doi:10.1126/science.1163886

Brovkina, O., Stojanović, M., Milanović, S., Latypov, I., Marković, N., & Cienciala, E. (2020). Monitoring of post-fire forest scars in Serbia based on satellite Sentinel-2 data. *Geomatics, Natural Hazards and Risk, 11*(1), 2315-2339. doi:10.1080/19475705.2020.1836037

Camia, A., Durrant, T., & San-Miguel-Ayanz, J. (2014). The European fire database: technical specifications and data submission. *EUR 26546 EN. Luxemburg (Luxemburg), Publications Office of the European Union*.

Certini, G. (2005). Effects of fire on properties of forest soils: a review. *Oecologia, 143*(1), 1-10.

Chas-Amil, M. L., Touza, J., & García-Martínez, E. (2013). Forest fires in the wildland–urban interface: A spatial analysis of forest fragmentation and human impacts. *Applied Geography, 43*, 127-137. doi:https://doi.org/10.1016/j.apgeog.2013.06.010

Chuvieco, E., Lizundia-Loiola, J., Pettinari, M. L., Ramo, R., Padilla, M., Tansey, K., . . . Heil, A. (2018). Generation and analysis of a new global burned area product based on MODIS 250 m reflectance bands and thermal anomalies. *Earth System Science Data, 10*(4), 2015-2031.

Chuvieco, E., Mouillot, F., van der Werf, G. R., San Miguel, J., Tanase, M., Koutsias, N., . . . Giglio, L. (2019). Historical background and current developments for mapping burned area from satellite Earth observation. *Remote Sensing of Environment, 225*, 45-64. doi:https://doi.org/10.1016/j.rse.2019.02.013

de Vos, N. (2018). *Inflammable ideas and contagious collaboration: a case study of the perception of wildfire risk and the production of wildfire mitigation policies on the Veluwe*. [Netherlands]: [publisher not identified].

Doerr, S. H., Santín, C., Maynard, T., Smith, N., & Gonzalez, S. (2013). *Wildfire: A burning issue for insurers?*

ESA. (2015). European Space Agency - Sentinel-2 User Handbook. Retrieved from https://sentinel.esa.int/documents/247904/685211/Sentinel-2_User_Handbook

Fernández-Manso, A., Fernández-Manso, O., & Quintano, C. (2016). SENTINEL-2A red-edge spectral indices suitability for discriminating burn severity. *International Journal of Applied Earth Observation and Geoinformation, 50*, 170-175. doi:https://doi.org/10.1016/j.jag.2016.03.005

Filipponi, F. (2018). *BAIS2: Burned Area Index for Sentinel-2* (Vol. 2).

Filipponi, F. (2019). Exploitation of sentinel-2 time series to map burned areas at the national level: A case study on the 2017 italy wildfires. *Remote Sensing, 11*(6), 622.

Filipponi, F., & Manfron, G. (2019). *Observing Post-Fire Vegetation Regeneration Dynamics Exploiting High-Resolution Sentinel-2 Data.* Paper presented at the Multidisciplinary Digital Publishing Institute Proceedings.

Flannigan, M., Cantin, A. S., de Groot, W. J., Wotton, M., Newbery, A., & Gowman, L. M. (2013). Global wildland fire season severity in the 21st century. *Forest Ecology and Management, 294*, 54-61. doi:https://doi.org/10.1016/j.foreco.2012.10.022

Flannigan, M. D., Stocks, B. J., & Wotton, B. M. (2000). Climate change and forest fires. *Science of the total environment, 262*(3), 221-229.

Giglio, L., Csiszar, I., & Justice, C. O. (2006). Global distribution and seasonality of active fires as observed with the Terra and Aqua Moderate Resolution Imaging Spectroradiometer (MODIS) sensors. *Journal of geophysical research: Biogeosciences, 111*(G2).

Govaerts, Y. M., Verstraete, M. M., Pinty, B., & Gobron, N. (1999). Designing optimal spectral indices: A feasibility and proof of concept study. *International Journal of Remote Sensing, 20*(9), 1853-1873. doi:10.1080/014311699212524

Hantson, S., Pueyo, S., & Chuvieco, E. (2015). Global fire size distribution is driven by human impact and climate. *Global Ecology and Biogeography, 24*(1), 77-86.

Hawthorne, D., & Mitchell, F. J. G. (2018). Investigating patterns of wildfire in Ireland and their correlation with regional and global trends in fire history. *Quaternary International, 488*, 58-66. doi:https://doi.org/10.1016/j.quaint.2017.06.067

Huang, H., Roy, D. P., Boschetti, L., Zhang, H. K., Yan, L., Kumar, S. S., . . . Li, J. (2016). Separability analysis of Sentinel-2A Multi-Spectral Instrument (MSI) data for burned area discrimination. *Remote Sensing, 8*(10), 873.

Huete, A. R. (2004). 11 - REMOTE SENSING FOR ENVIRONMENTAL MONITORING. In J. F. Artiola, I. L. Pepper, & M. L. Brusseau (Eds.), *Environmental Monitoring and Characterization* (pp. 183-206). Burlington: Academic Press.

Jupudi, L. (2018). Machine learning techniques using python for data analysis in performance evaluation. *International Journal of Intelligent Systems Technologies and Applications, 17*, 3. doi:10.1504/IJISTA.2018.091584

Key, C., & Benson, N. (2006). Landscape Assessment: Ground measure of severity, the Composite Burn Index; and Remote sensing of severity, the Normalized Burn Ratio. In (pp. LA 1-51).

Khabarov, N., Krasovskii, A., Obersteiner, M., Swart, R., Dosio, A., San-Miguel-Ayanz, J., . . . Migliavacca, M. (2016). Forest fires and adaptation options in Europe. *Regional Environmental Change, 16*(1), 21-30.

Lacouture, D. L., Broadbent, E. N., & Crandall, R. M. (2020). Detecting Vegetation Recovery after Fire in A Fire-Frequented Habitat Using Normalized Difference Vegetation Index (NDVI). *Forests, 11*(7), 749.

Lasaponara, R. (2006). Estimating spectral separability of satellite derived parameters for burned areas mapping in the Calabria region by using SPOT-Vegetation data. *Ecological Modelling, 196*(1-2), 265-270.

Lasaponara, R., Proto, A. M., Aromando, A., Cardettini, G., Varela, V., & Danese, M. (2020). On the Mapping of Burned Areas and Burn Severity Using Self Organizing Map and Sentinel-2 Data. *IEEE Geoscience and Remote Sensing Letters, 17*(5), 854-858. doi:10.1109/LGRS.2019.2934503

Lentile, L., Holden, Z., Smith, A., Falkowski, M., Hudak, A. T., Morgan, P., . . . Benson, N. (2006). Remote sensing techniques to assess active fire characteristics and post-fire effects. *International Journal of Wildland Fire, 15*. doi:10.1071/WF05097

Marlier, M., DeFries, R., Voulgarakis, A., Kinney, P., Randerson, J., Shindell, D., . . . Faluvegi, G. (2013). El Niño and health risks from landscape fire emissions in Southeast Asia. *Nature Climate Change, 3*, 131 - 136.

Mathu, L. F. A. (2020). How soil texture and groundwater level drive wildfire occurrence in North-western Europe. *Wageningen University & Research, Wageningen (NL)*.

Meng, Y., Deng, Y., & Shi, P. (2015). Mapping forest wildfire risk of the world. In *World Atlas of Natural Disaster Risk* (pp. 261-275): Springer.

Modugno, S., Balzter, H., Cole, B., & Borrelli, P. (2016). Mapping regional patterns of large forest fires in Wildland–Urban Interface areas in Europe. *Journal of Environmental Management, 172*, 112-126. doi:https://doi.org/10.1016/j.jenvman.2016.02.013

Moritz, M. A., Parisien, M.-A., Batllori, E., Krawchuk, M. A., Van Dorn, J., Ganz, D. J., & Hayhoe, K. (2012). Climate change and disruptions to global fire activity. *Ecosphere, 3*(6), art49. doi:10.1890/es11-00345.1

OECD. (2020). Population indicator. Retrieved from https://data.oecd.org/pop/population.htm

Pettinari, M. L., & Chuvieco, E. (2020). Fire Danger Observed from Space. *Surveys in Geophysics*, 1-23.

Randerson, J., Chen, Y., Werf, G., Rogers, B., & Morton, D. (2012). Global burned area and biomass burning emissions from small fires. *Journal of geophysical research: Biogeosciences, 117*, G04012. doi:10.1029/2012jg002128

Ranghetti, L., Boschetti, M., Nutini, F., & Busetto, L. (2020). "sen2r": An R toolbox for automatically downloading and preprocessing Sentinel-2 satellite data. *Computers & Geosciences, 139*, 104473. doi:https://doi.org/10.1016/j.cageo.2020.104473

Rooij, L. L. d., Stoof, C. R., & Agricola, H. J. (2020). *Klimaatschadeschatter Rapportage 2020 : Bestrijdingskosten van Natuurbranden*. Retrieved from Bussum: https://edepot.wur.nl/537827

Roteta, E., Bastarrika, A., Padilla, M., Storm, T., & Chuvieco, E. (2019). Development of a Sentinel-2 burned area algorithm: Generation of a small fire database for sub-Saharan Africa. *Remote Sensing of Environment, 222*, 1-17.

San-Miguel-Ayanz, Durrant, T., Boca, R., Libertà, G., Branco, A., de Rigo, D., . . . Schulte, E. (2018). Forest Fires in Europe, Middle East and North Africa. In: EUR.

San-Miguel-Ayanz, Schulte, E., Schmuck, G., Camia, A., Strobl, P., Liberta, G., . . . Kempeneers, P. (2012). Comprehensive monitoring of wildfires in Europe: the European forest fire information system (EFFIS). In *Approaches to managing disaster-Assessing hazards, emergencies and disaster impacts*: IntechOpen.

San-Miguel-Ayanz, J., Durrant, T., Boca, R., Libertà, G., Branco, A., de Rigo, D., . . . Villa Juan, J. D. (2019). *Forest fires in Europe, Middle East and North Africa 2018*.

Schroeder, W., Oliva, P., Giglio, L., Quayle, B., Lorenz, E., & Morelli, F. (2016). Active fire detection using Landsat-8/OLI data. *Remote Sensing of Environment, 185*, 210-220. doi:https://doi.org/10.1016/j.rse.2015.08.032

Smeenk, A. (2011). Kennisplein-Dutch Thematic Publication Wildfires: The 15 Most Frequently Asked Questions. Retrieved April 2, 2016. In.

Smiraglia, D., Filipponi, F., Mandrone, S., Antonella, T., & Taramelli, A. (2020). Agreement Index for Burned Area Mapping: Integration of Multiple Spectral Indices Using Sentinel-2 Satellite Images. *Remote Sensing, 12*, 1862. doi:10.3390/rs12111862

Stoof, C. (2020). Nature Today - Nederland moet leren leven met vuur. Retrieved from https://www.naturetoday.com/intl/nl/nature-reports/message/?msg=26471

Stoof, C., Moore, D., Fernandes, P. M., Stoorvogel, J. J., Fernandes, R. E. S., Ferreira, A. J. D., & Ritsema, C. J. (2013). Hot fire, cool soil. *Geophysical Research Letters, 40*(8), 1534-1539. doi:https://doi.org/10.1002/grl.50299

Stoof, C. R., Tavia, V. M., Marcotte, A. L., Stoorvogel, J. J., & Ribau, M. C. (2020). *Relatie tussen natuurbeheer en brandveiligheid in de Deurnese Peel: onderzoek naar aanleiding van de brand in de Deurnese Peel van 20 april 2020*. Retrieved from

Tedim, F., Xanthopoulos, G., & Leone, V. (2015). Forest fires in Europe: Facts and challenges wildfire. Hazards, risks, and disasters, 1, 5. In: Elsevier: Douglas Paton.

Tepley, A. J., Thomann, E., Veblen, T. T., Perry, G. L., Holz, A., Paritsis, J., . . . Anderson-Teixeira, K. J. (2018). Influences of fire–vegetation feedbacks and post-fire recovery rates on forest landscape vulnerability to altered fire regimes. *Journal of Ecology, 106*(5), 1925-1940.

van Dijk, D., Shoaie, S., van Leeuwen, T., & Veraverbeke, S. (2021). Spectral signature analysis of false positive burned area detection from agricultural harvests using Sentinel-2 data. *International Journal of Applied Earth Observation and Geoinformation, 97*, 102296. doi:https://doi.org/10.1016/j.jag.2021.102296

Viana-Soto, A., Aguado, I., & Martínez, S. (2017). Assessment of post-fire vegetation recovery using fire severity and geographical data in the mediterranean region (Spain). *Environments, 4*(4), 90.

Vilar, L., Camia, A., & San-Miguel-Ayanz, J. (2015). A comparison of remote sensing products and forest fire statistics for improving fire information in Mediterranean Europe. *European Journal of Remote Sensing, 48*(1), 345-364. doi:10.5721/EuJRS20154820

Wang, S., Baig, M. H. A., Liu, S., Wan, H., Wu, T., & Yang, Y. (2018). Estimating the area burned by agricultural fires from Landsat 8 Data using the Vegetation Difference Index and Burn Scar Index. *International Journal of Wildland Fire, 27*(4), 217-227. doi:https://doi.org/10.1071/WF17069

Weirather, M., Zeug, G., & Schneider, T. Automated Delineation Of Wildfire Areas Using Sentinel-2 Satellite Imagery. *GI_Forum 2018, 6*, 251-262.

Weirather, M., Zeug, G., & Schneider, T. (2018). Automated Delineation Of Wildfire Areas Using Sentinel-2 Satellite Imagery. *GI_Forum, 1*, 251-262. doi:10.1553/giscience2018_01_s251

Yang, J., He, H. S., Shifley, S. R., & Gustafson, E. J. (2007). Spatial patterns of modern period human-caused fire occurrence in the Missouri Ozark Highlands. *Forest science, 53*(1), 1-15.

APPENDIX I – SCRIPT WORKFLOW IN ERDAS

<u>NBR</u>
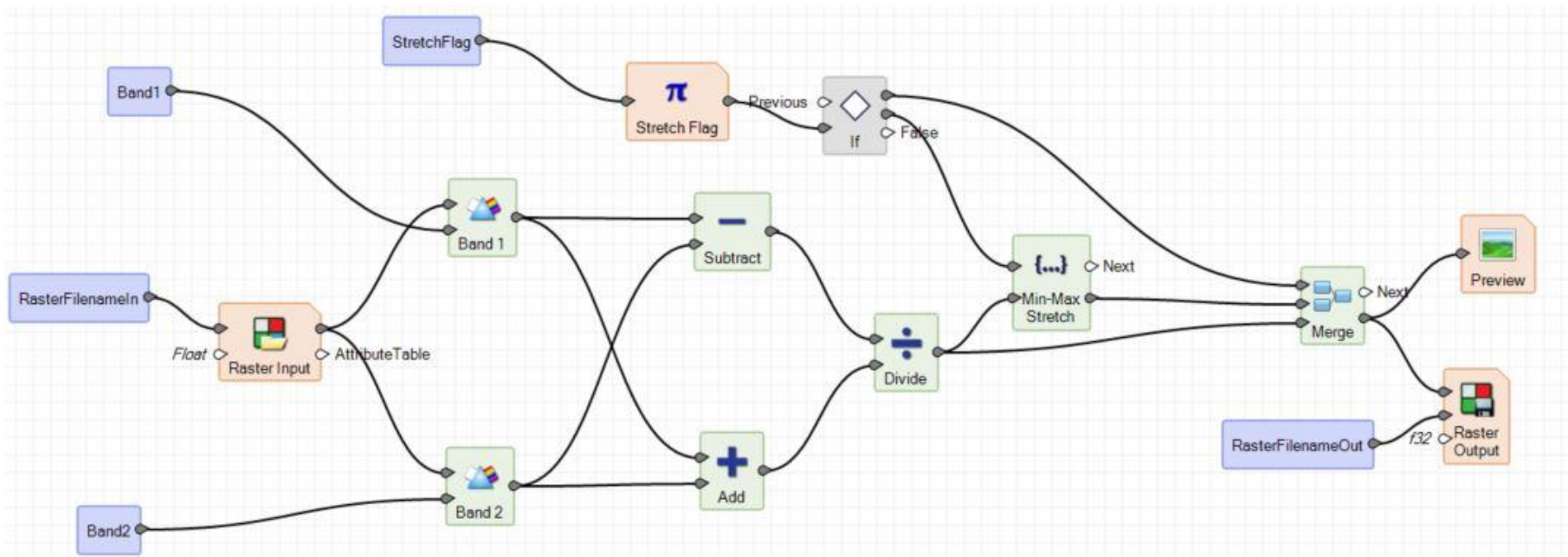
NDVI
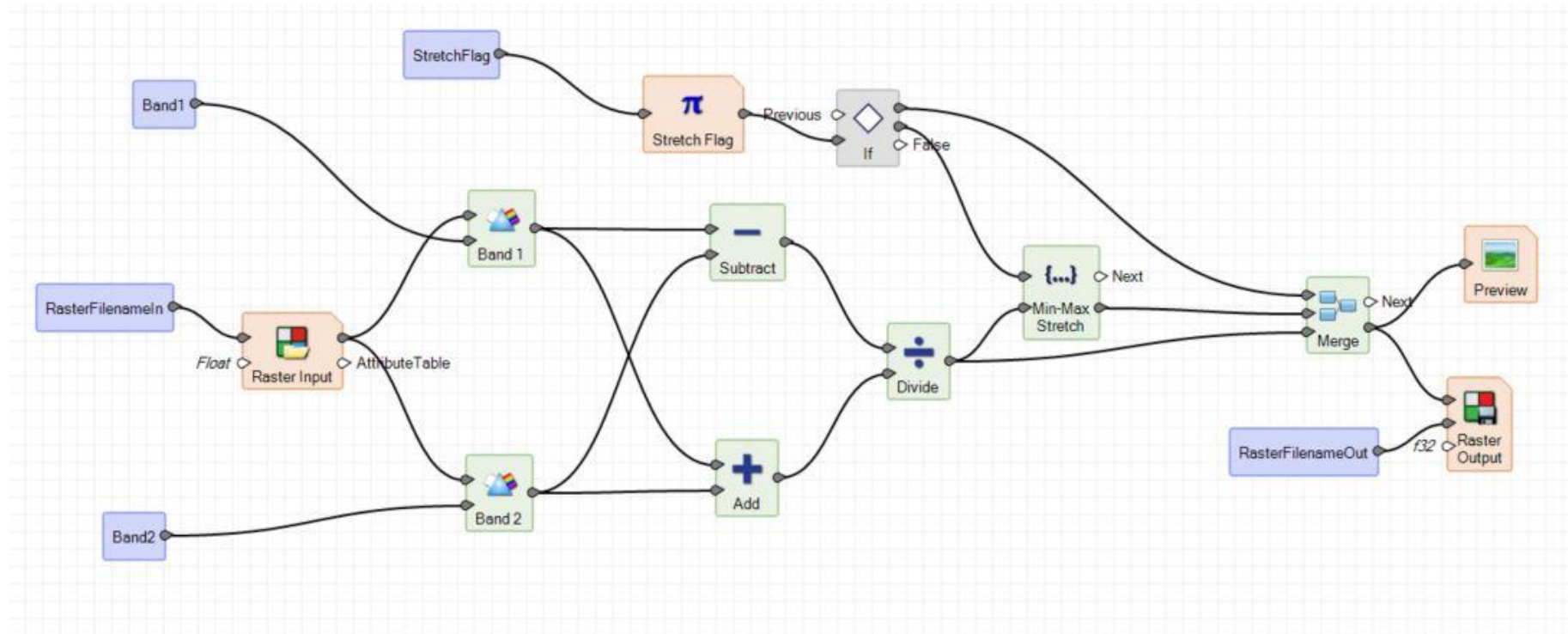
BAIS2

dNBR

APPENDIX II – LIST OF STUDIED FIRE EVENTS

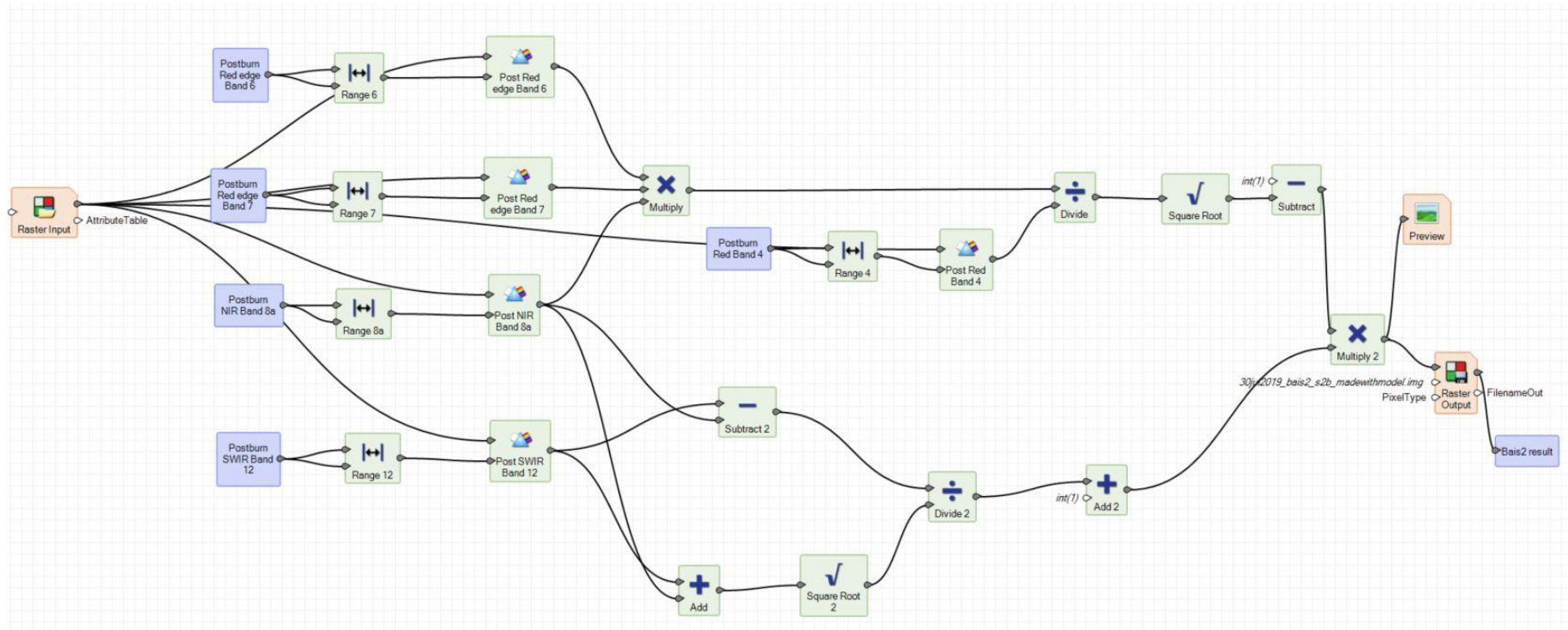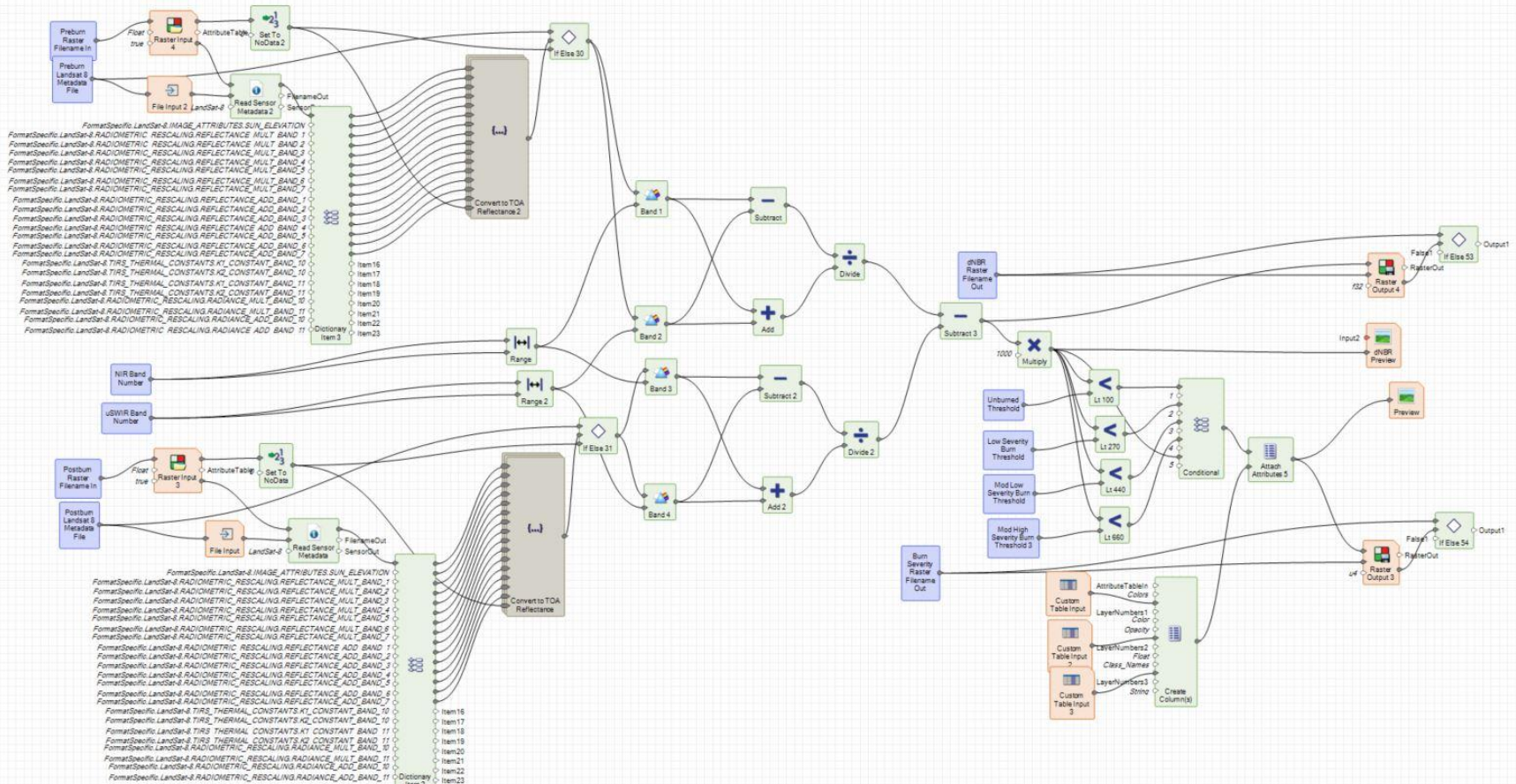| FIREID	ADD_LOCATI	CITY	DATEAL	Burned_total (ha)	Class_CAUSE_EU	Land_Cover
2018_0010	Beekhuizenseweg	Rheden	18/02/2018	0.02	Deliberate	Heide
2018_0013	Apeldoornseweg	Hoenderloo	26/02/2018	1	Negligence	Heide
2018_0018	Deurnesche Maria Peel	Liessel	28/02/2018	70	Deliberate	Grassland
2018_0020	Eperweg	't Harde	28/02/2018	2	Accident	Heide
2018_0021	Imkerweg	Helenaveen	01/03/2018	15	Deliberate	Grassland
2018_0026	Lagebrugweg	Helenaveen	05/03/2018	15	Deliberate	Grassland
2018_0061	Huisvenseweg	Heeze	14/04/2018	1	Unknown	Forest
2018_0066	Huyerenseweg	Tubbergen	18/04/2018	25	Unknown	Forest
2018_0067	Elspeterbosweg	Vierhouten	18/04/2018	4	Deliberate	Heide
2018_0073	Zoom	Assen	20/04/2018	2	Deliberate	Heide
2018_0078	Strabrechtse Heide	Heeze	21/04/2018	10	Unknown	Heide
2018_0083	Zoom	Assen	21/04/2018	2	Rekindle	Heide
2018_0088	Steenweg	Ter Apel	22/04/2018	2	Unknown	Forest
2018_0104	Ginkelsche Heide	Ede	07/05/2018	7	Accident	Heide
2018_0140	Heidepolweg	Vorden	24/05/2018	6	Deliberate	Heide
2018_0171	Eperweg	't Harde	19/06/2018	2.5	Accident	Heide
2018_0190	Oranjeweg	Zuid-Beijerland	28/06/2018	2	Unknown	Grassland
2018_0195	Middelsteeg	Beugen	28/06/2018	2	Unknown	Grassland
2018_0210	Mastendreef	Bergen op Zoom	30/06/2018	4	Deliberate	Heide
2018_0214	Molenweg	Wedde	30/06/2018	15	Accident	Grassland
2018_0224	Broekweg	Montfort	30/06/2018	1	Unknown	Grassland
2018_0226	Fabrieksstraat	Budel-Dorplein	01/07/2018	12	Deliberate	Grassland
2018_0261	De Leuke	Vorden	02/07/2018	1	Accident	Grassland
2018_0263	Noorddijk	Zuid-Beijerland	02/07/2018	1	Accident	Grassland
2018_0276	De Siptenpad	Tilburg	03/07/2018	1	Unknown	Forest
2018_0327	Dalmsholterweg	Dalfsen	07/07/2018	3	Deliberate	Heide
2018_0365	Breelaan	Bergen (NH)	11/07/2018	1	Unknown	Grassland
2018_0387	Philipsweg	Maarheeze	14/07/2018	3	Deliberate	Forest
2018_0400	Gebroekerdijk	Echt	15/07/2018	4	Unknown	Grassland
2018_0417	Kruisberg	Heemskerk	16/07/2018	2	Unknown	Grassland
2018_0422	Molenweg	Wedde	16/07/2018	4	Accident	Grassland
2018_0486	Hooiweg	Elspeet	20/07/2018	6	Unknown	Heide
2018_0487	Zwarteweg	Beerze	20/07/2018	5	Accident	Forest
2018_0548	Sportlaan	Boxmeer	25/07/2018	3	Deliberate	Forest
2018_0553	Piet van Bokhovenpad	Helmond	25/07/2018	4	Unknown	Grassland
2018_0566	Sterkselseweg	Maarheeze	26/07/2018	16	Deliberate	Forest
2018_0568	Torenstreek	Schiermonnikoog	26/07/2018	1.5	Deliberate	Grassland
2018_0637	Mastendreef	Bergen op Zoom	31/07/2018	2	Deliberate	Heide
2018_0644	Buurserstraat	Enschede	31/07/2018	1	Deliberate	Grassland
2018_0692	Ebbenstraat	Lomm	04/08/2018	9	Deliberate	Grassland
2018_0703	Fransebaan	Alphen	05/08/2018	4	Unknown	Heide
2018_0778	Brouwersdam	Ouddorp	16/08/2018	1	Deliberate	Grassland
2018_0817	Heumensebaan	Molenhoek	31/08/2018	3		
2018_0885	Eperweg	't Harde	08/10/2018	4	Accident	Heide
2018_0886	Eperweg	't Harde	08/10/2018	2.5	Accident	Heide

2018_0900	Eperweg	't Harde	10/10/2018	1	Accident	Heide
2018_0901	Eperweg	't Harde	10/10/2018	3.5	Accident	Heide
2018_0923	Eperweg	't Harde	16/10/2018	1	Accident	Heide
2018_0927	Eperweg	't Harde	17/10/2018	2	Accident	Heide
2019_0018	Woldlakeweg	Scheerwolde	01/04/2019	1	Deliberate	Grasland
2019_0021	Gasthuisdijk	Wanneperveen	04/04/2019	1	Deliberate	Grasland
2019_0024	Prins Hendriklaan	Lage Mierde	07/04/2019	5	Deliberate	Forest
2019_0030	Gemertseweg	Oploo	09/04/2019	2	Deliberate	Forest
2019_0031	Clement van Maasdijklaan	Arnhem	10/04/2019	15	Accident	Grasland
2019_0032	Beekakkersweg	Lage Mierde	10/04/2019	1	Deliberate	Heide
2019_0034	Torenlaan	Drunen	11/04/2019	8	Deliberate	Forest
2019_0044	Zwartven	Hooge Mierde	15/04/2019	2	Deliberate	Forest
2019_0051	Maarschalkersteeg	Soest	18/04/2019	4	Deliberate	Forest
2019_0052	Engelberterweg	Groningen	18/04/2019	10	Unknown	Grasland
2019_0073	Korenburgerveenweg	Winterswijk	20/04/2019	4	Unknown	Grasland
2019_0084	Sambeeksedijk	Sambeek	20/04/2019	4	Deliberate	Forest
2019_0092	Kruisberglaan	De Rips	21/04/2019	4	Deliberate	Forest
2019_0105	Sint Walrickweg	Wijchen	22/04/2019	1	Unknown	Grasland
2019_0122	Onderveldsweg	Diffelen	23/04/2019	1	Unknown	Forest
2019_0533	Eperweg	t Harde	23/04/2019	7.5	Accident	Heide
2019_0135	Piet van Bokhovenpad	Helmond	24/04/2019	1	Deliberate	Grasland
2019_0156	Van Manenspad	Epe	13/05/2019	22	Deliberate	Heide
2019_0160	Kolonel H. L. van Royenweg	Leusden	15/05/2019	25	Accident	Heide
2019_0218	Peter van den Breemerweg	Soest	26/06/2019	1	Unknown	Grasland
2019_0271	Putterweg	Voerendaal	06/07/2019	1	Unknown	Grasland
2019_0554	Eperweg	t Harde	17/07/2019	2	Accident	Heide
2019_0295	Eperweg	t Harde	18/07/2019	15	Accident	Heide
2019_0301	Munnekeveld	Wijchen	22/07/2019	1	Deliberate	Heide
2019_0303	Hei	Kessel	23/07/2019	2	Accident	Grasland
2019_0316	Malderburchtstraat	Nijmegen	24/07/2019	2	Negligence	Grasland
2019_0325	Cortenbacherveldweg	Voerendaal	25/07/2019	1	Unknown	Grasland
2019_0326	Vreehorstweg	Winterswijk	25/07/2019	26	Accident	Grasland
2019_0327	Oude Nieuwlandseweg	Nieuwerkerk	25/07/2019	3	Unknown	Grasland
2019_0334	Bosbergstraat	Lomm	26/07/2019	3	Unknown	Grasland
2019_0337	Nummerlaan	Blijham	27/07/2019	15	Accident	Grasland
2019_0344	Kuilenweg	Bruchterveld	27/07/2019	2	Accident	Grasland
2019_0346	Oranje	Oranje	28/07/2019	10	Accident	Grasland
2019_0349	Ooijmanlaan	Doetinchem	29/07/2019	2	Unknown	Grasland
2019_0351	Stakenbergweg	Elspeet	30/07/2019	1	Deliberate	Heide
2019_0354	Lekdijk West	Wijk bij Duurstede	30/07/2019	3	Accident	Grasland
2019_0398	Postweg	Vlieland	02/09/2019	13	Accident	Grasland
2019_0406	Heuvel	Budel	15/09/2019	1	Deliberate	Forest
2020_04	Deurnese Peel	De Peel	20/04/2020	700	Unknown	Grassland

APPENDIX III – SENTINEL-2 IMAGES

S2A_MSIL1C_20180207T104211_N0206_R008_T31UFT_20180207T124633	S2B_MSIL2A_20180712T104019_N0208_R008_T31UGU_20180712T150813
S2A_MSIL1C_20180302T105021_N0206_R051_T31UFU_20180302T130434	S2B_MSIL2A_20180712T104019_N0208_R008_T32ULD_20180712T150813
S2A_MSIL1C_20180418T104021_N0206_R008_T31UFT_20180418T125356	S2B_MSIL2A_20180715T105029_N0208_R051_T31UET_20180715T152821
S2A_MSIL1C_20180418T104021_N0206_R008_T31UFU_20180418T125356	S2B_MSIL2A_20180715T105029_N0208_R051_T31UFS_20180715T152821
S2A_MSIL1C_20180418T104021_N0206_R008_T32ULD_20180418T125356	S2B_MSIL2A_20180715T105029_N0208_R051_T31UFT_20180715T152821
S2A_MSIL1C_20180421T105031_N0206_R051_T31UFU_20180421T111316	S2B_MSIL2A_20180715T105029_N0208_R051_T31UFU_20180715T152821
S2A_MSIL1C_20180421T105031_N0206_R051_T31UGU_20180421T111316	S2B_MSIL2A_20180715T105029_N0208_R051_T31UGT_20180715T152821
S2A_MSIL1C_20180421T105031_N0206_R051_T32ULD_20180421T111316	S2B_MSIL2A_20180715T105029_N0208_R051_T31UGU_20180715T152821
S2A_MSIL1C_20180508T104031_N0206_R008_T31UFT_20180508T175127	S2B_MSIL2A_20180715T105029_N0208_R051_T32ULD_20180715T152821
S2A_MSIL1C_20180521T105031_N0206_R051_T31UGT_20180521T111327	S2B_MSIL2A_20180722T104019_N0208_R008_T31UFS_20180722T150416
S2A_MSIL2A_20180227T104021_N0206_R008_T31UFT_20180227T141612	S2B_MSIL2A_20180722T104019_N0208_R008_T31UGS_20180722T150416
S2A_MSIL2A_20180418T104021_N0207_R008_T31UFT_20180418T125356	S2B_MSIL2A_20180804T105019_N0208_R051_T31UET_20180804T153639
S2A_MSIL2A_20180421T105031_N0207_R051_T31UFT_20180421T125911	S2B_MSIL2A_20180807T105619_N0208_R094_T31UET_20180807T162012
S2A_MSIL2A_20180508T104031_N0207_R008_T31UFT_20180508T175127	S2B_MSIL2A_20180814T105019_N0208_R051_T31UGU_20180814T164728
S2A_MSIL2A_20180531T105031_N0208_R051_T31UGU_20180531T144336	S2B_MSIL2A_20180817T105619_N0208_R094_T31UET_20180817T171259
S2A_MSIL2A_20180607T104021_N0208_R008_T31UFU_20180607T132721	S2B_MSIL2A_20181010T104019_N0209_R008_T31UFT_20181010T171128
S2A_MSIL2A_20180620T105031_N0208_R051_T31UGU_20180620T165727	S2B_MSIL2A_20181010T104019_N0209_R008_T31UFU_20181010T171128
S2A_MSIL2A_20180627T104021_N0208_R008_T31UFT_20180627T134546	S2B_MSIL2A_20181013T105029_N0209_R051_T31UFT_20181013T154254
S2A_MSIL2A_20180627T104021_N0208_R008_T31UFU_20180627T134546	S2B_MSIL2A_20181013T105029_N0209_R051_T31UFU_20181013T154254
S2A_MSIL2A_20180627T104021_N0208_R008_T31UGS_20180627T134546	S2A_MSIL2A_20190423T104031_N0211_R008_T31UGU_20190423T133421
S2A_MSIL2A_20180627T104021_N0208_R008_T31UGU_20180627T134546	S2A_MSIL2A_20190423T104031_N0211_R008_T32ULC_20190423T133421
S2A_MSIL2A_20180627T104021_N0208_R008_T32ULC_20180627T134546	S2A_MSIL2A_20190423T104031_N0211_R008_T32ULD_20190423T133421
S2A_MSIL2A_20180627T104021_N0208_R008_T32ULD_20180627T134546	S2A_MSIL2A_20190513T104031_N0212_R008_T31UFT_20190513T134155
S2A_MSIL2A_20180630T105031_N0208_R051_T31UET_20180630T144133	S2A_MSIL2A_20190513T104031_N0212_R008_T31UFU_20190513T134155
S2A_MSIL2A_20180630T105031_N0208_R051_T31UFS_20180630T144133	S2A_MSIL2A_20190513T104031_N0212_R008_T31UGT_20190513T134155
S2A_MSIL2A_20180630T105031_N0208_R051_T31UFT_20180630T144133	S2A_MSIL2A_20190513T104031_N0212_R008_T31UGU_20190513T134155
S2A_MSIL2A_20180630T105031_N0208_R051_T31UFU_20180630T144133	S2A_MSIL2A_20190523T104031_N0212_R008_T31UFT_20190523T132214
S2A_MSIL2A_20180707T104021_N0208_R008_T31UFS_20180707T140903	S2A_MSIL2A_20190523T104031_N0212_R008_T31UGT_20190523T132214
S2A_MSIL2A_20180707T104021_N0208_R008_T31UGS_20180707T140903	S2A_MSIL2A_20190602T104031_N0212_R008_T31UFT_20190602T140340
S2A_MSIL2A_20180707T104021_N0208_R008_T31UGT_20180707T140903	S2A_MSIL2A_20190602T104031_N0212_R008_T31UFU_20190602T140340
S2A_MSIL2A_20180707T104021_N0208_R008_T32ULC_20180707T140903	S2A_MSIL2A_20190625T105031_N0212_R051_T31UFU_20190625T134744
S2A_MSIL2A_20180717T104021_N0208_R008_T31UFT_20180717T164745	S2A_MSIL2A_20190625T105031_N0212_R051_T32ULD_20190625T134744
S2A_MSIL2A_20180717T104021_N0208_R008_T31UFU_20180717T164745	S2A_MSIL2A_20190702T104031_N0212_R008_T31UFT_20190702T135726
S2A_MSIL2A_20180717T104021_N0208_R008_T31UGT_20180717T164745	S2A_MSIL2A_20190705T105031_N0212_R051_T31UET_20190705T140734
S2A_MSIL2A_20180717T104021_N0208_R008_T32ULD_20180717T164745	S2A_MSIL2A_20190722T104031_N0213_R008_T31UFT_20190722T120459
S2A_MSIL2A_20180717T104021_N0208_R008_T32ULE_20180717T164745	S2A_MSIL2A_20190725T105031_N0213_R051_T31UFT_20190725T132538
S2A_MSIL2A_20180720T105031_N0208_R051_T31UFS_20180720T135744	S2A_MSIL2A_20190725T105031_N0213_R051_T31UFU_20190725T132538
S2A_MSIL2A_20180720T105031_N0208_R051_T31UFT_20180720T135744	S2A_MSIL2A_20190725T105031_N0213_R051_T31UGS_20190725T132538
S2A_MSIL2A_20180720T105031_N0208_R051_T31UFU_20180720T135744	S2A_MSIL2A_20190725T105031_N0213_R051_T31UGT_20190725T132538
S2A_MSIL2A_20180720T105031_N0208_R051_T31UGU_20180720T135744	S2A_MSIL2A_20190804T105031_N0213_R051_T31UGS_20190804T132247
S2A_MSIL2A_20180727T104021_N0208_R008_T31UFS_20180727T134459	S2A_MSIL2A_20190814T105031_N0213_R051_T31UFT_20190814T120854

S2A_MSIL2A_20180727T104021_N0208_R008_T31UFT_20180727T134459	S2A_MSIL2A_20190824T105031_N0213_R051_T31UFT_20190824T134703
S2A_MSIL2A_20180727T104021_N0208_R008_T31UFU_20180727T134459	S2A_MSIL2A_20190824T105031_N0213_R051_T31UFU_20190824T134703
S2A_MSIL2A_20180727T104021_N0208_R008_T31UGT_20180727T134459	S2A_MSIL2A_20190824T105031_N0213_R051_T31UFV_20190824T134703
S2A_MSIL2A_20180727T104021_N0208_R008_T31UGU_20180727T134459	S2A_MSIL2A_20190831T104021_N0213_R008_T31UFS_20190831T140616
S2A_MSIL2A_20180727T104021_N0208_R008_T32ULC_20180727T134459	S2A_MSIL2A_20190831T104021_N0213_R008_T31UFT_20190831T140616
S2A_MSIL2A_20180727T104021_N0208_R008_T32ULD_20180727T134459	S2A_MSIL2A_20190913T105031_N0213_R051_T31UFV_20190913T120946
S2A_MSIL2A_20180727T104021_N0208_R008_T32ULE_20180727T134459	S2A_MSIL2A_20190920T104021_N0213_R008_T31UFS_20190920T120330
S2A_MSIL2A_20180806T104021_N0208_R008_T31UFT_20180806T142805	S2B_MSIL2A_20190329T104029_N0211_R008_T31UGU_20190329T164503
S2A_MSIL2A_20180806T104021_N0208_R008_T31UGT_20180806T142805	S2B_MSIL2A_20190401T105029_N0211_R051_T31UFS_20190401T140125
S2A_MSIL2A_20180806T104021_N0208_R008_T31UGU_20180806T142805	S2B_MSIL2A_20190401T105029_N0211_R051_T31UFT_20190401T140125
S2A_MSIL2A_20180806T104021_N0208_R008_T32ULC_20180806T142805	S2B_MSIL2A_20190408T104029_N0211_R008_T31UFT_20190408T135037
S2A_MSIL2A_20180918T105021_N0208_R051_T31UFT_20180918T141223	S2B_MSIL2A_20190408T104029_N0211_R008_T31UGU_20190408T135037
S2A_MSIL2A_20181005T104021_N0208_R008_T31UFU_20181007T220806	S2B_MSIL2A_20190418T104029_N0211_R008_T31UFS_20190418T135653
S2A_MSIL2A_20181028T105141_N0209_R051_T31UFU_20181028T135837	S2B_MSIL2A_20190418T104029_N0211_R008_T31UFT_20190418T135653
S2A_MSIL2A_20181114T104301_N0210_R008_T31UFT_20181114T140426	S2B_MSIL2A_20190418T104029_N0211_R008_T31UFU_20190418T135653
S2A_MSIL2A_20181117T105321_N0210_R051_T31UFT_20181117T121932	S2B_MSIL2A_20190418T104029_N0211_R008_T32ULC_20190418T135653
S2B_MSIL1C_20180222T104029_N0206_R008_T31UFT_20180223T170250	S2B_MSIL2A_20190421T105039_N0211_R051_T31UFT_20190421T133439
S2B_MSIL1C_20180222T104029_N0206_R008_T31UGT_20180223T170250	S2B_MSIL2A_20190421T105039_N0211_R051_T31UFU_20190421T133439
S2B_MSIL1C_20180225T105019_N0206_R051_T31UFU_20180225T143259	S2B_MSIL2A_20190518T104029_N0212_R008_T31UFT_20190518T135927
S2B_MSIL1C_20180406T105029_N0206_R051_T31UFT_20180406T125448	S2B_MSIL2A_20190518T104029_N0212_R008_T31UGT_20190518T135927
S2B_MSIL1C_20180406T105029_N0206_R051_T31UFU_20180406T125448	S2B_MSIL2A_20190607T104029_N0212_R008_T31UFT_20190607T135245
S2B_MSIL1C_20180406T105029_N0206_R051_T31UGU_20180406T125448	S2B_MSIL2A_20190627T104029_N0212_R008_T31UFT_20190627T135004
S2B_MSIL1C_20180506T105029_N0206_R051_T31UFT_20180509T155709	S2B_MSIL2A_20190627T104029_N0212_R008_T31UGS_20190627T135004
S2B_MSIL1C_20180506T105029_N0206_R051_T32ULD_20180509T155709	S2B_MSIL2A_20190627T104029_N0212_R008_T32ULC_20190627T135004
S2B_MSIL1C_20180513T104019_N0206_R008_T31UFT_20180513T114818	S2B_MSIL2A_20190717T104029_N0213_R008_T31UFT_20190717T151314
S2B_MSIL1C_20180526T105029_N0206_R051_T31UGT_20180526T134138	S2B_MSIL2A_20190717T104029_N0213_R008_T31UFU_20190717T151314
S2B_MSIL2A_20180304T104019_N0206_R008_T31UFT_20180304T142412	S2B_MSIL2A_20190727T104029_N0213_R008_T31UGT_20190727T134640
S2B_MSIL2A_20180314T104019_N0206_R008_T31UFT_20180314T142720	S2B_MSIL2A_20190727T104029_N0213_R008_T32ULC_20190727T134640
S2B_MSIL2A_20180506T105029_N0207_R051_T31UFT_20180509T155709	S2B_MSIL2A_20190727T104029_N0213_R008_T32ULD_20190727T134640
S2B_MSIL2A_20180526T105029_N0208_R051_T31UET_20180526T141411	S2B_MSIL2A_20190730T105039_N0213_R051_T31UET_20190730T140936
S2B_MSIL2A_20180702T104019_N0208_R008_T31UFS_20180702T150728	S2B_MSIL2A_20190730T105039_N0213_R051_T31UFT_20190730T140936
S2B_MSIL2A_20180702T104019_N0208_R008_T31UFT_20180702T150728	S2B_MSIL2A_20190730T105039_N0213_R051_T31UGS_20190730T140936
S2B_MSIL2A_20180702T104019_N0208_R008_T31UGS_20180702T150728	S2B_MSIL2A_20190730T105039_N0213_R051_T31UGT_20190730T140936
S2B_MSIL2A_20180702T104019_N0208_R008_T31UGU_20180702T150728	S2B_MSIL2A_20190730T105039_N0213_R051_T32ULD_20190730T140936
S2B_MSIL2A_20180702T104019_N0208_R008_T32ULC_20180702T150728	S2B_MSIL2A_20190826T104029_N0213_R008_T32ULC_20190826T140844
S2B_MSIL2A_20180702T104019_N0208_R008_T32ULD_20180702T150728	S2B_MSIL2A_20190826T104029_N0213_R008_T32ULD_20190826T140844
S2B_MSIL2A_20180705T105029_N0208_R051_T31UET_20180705T152258	S2B_MSIL2A_20190905T104029_N0213_R008_T31UFT_20190905T135151
S2B_MSIL2A_20180705T105029_N0208_R051_T31UFT_20180705T152258	S2B_MSIL2A_20200422T103619_N0214_R008_T31UFT_20200422T140230
S2B_MSIL2A_20180712T104019_N0208_R008_T31UFT_20180712T150813	S2A_MSIL2A_20200420T105031_N0214_R051_T31UFT_20200420T134306
S2B_MSIL2A_20180712T104019_N0208_R008_T31UFU_20180712T150813	S2A_MSIL2A_20200417T104021_N0214_R008_T31UFT_20200417T112906
S2B_MSIL2A_20180712T104019_N0208_R008_T31UGT_20180712T150813	

APPENDIX IV – R SCRIPT RESEARCH QUESTION 2

```
# Mariana Diniz Silvestre
# Feel free to use, modify, and share

###

setwd("C:\\Users\\your_directory")

# Loading packages
if(!require(data.table)) install.packages("data.table ", dep=T); library(data.table)
if(!require(tidyverse)) install.packages("tidyverse", dep=T); library(tidyverse)
if(!require(lubridate)) install.packages("lubridate ", dep=T); library(lubridate)
if(!require(reshape)) install.packages("reshape", dep=T); library(reshape)
if(!require(extrafont)) install.packages("extrafont", dep=T); library(extrafont)

# Reading the data
images<-read.csv("images_total.csv", sep = ",", head = T, na.strings = "")
head(images)
str(images)
test<-images[duplicated(images),]  #no repeated line

# Converting date columns
images$Img_DATE_pre<-ymd(substr(images$Img_DATE_pre, 1, 10))
images$Img_DATE_post<-ymd(substr(images$Img_DATE_post, 1, 10))
images$DATEAL<-ymd(substr(images$DATEAL, 1, 10))

head(images)
str(images)

###Research Question 2###

# Including information about month and season
#images$year<-as.numeric(substr(images$DATEAL, 1, 4))
images$month<-as.numeric(substr(images$DATEAL, 6, 7))
images$season<-ifelse(images$month %in% 3:5, "spring", ifelse(images$month %in% 6:8, "summer",
                 ifelse(images$month %in%9:11, "fall", "winter")))
head(images)

# Checking the positive detection
images_yes <- images %>% filter(dNBR_Id == "yes")
head(images_yes)

#Grouping for months
images_yes %>% group_by(month) %>% tally()

#Combining by season
season<- as.data.frame(images_yes %>% group_by(season) %>% tally()) season
seas_ord<-c("spring", "summer", "fall", "winter")
tiff(file = "001_Detected_Fires_season.tiff", width = 3200, height = 1600, units = "px", res = 300)
s <- ggplot(season, aes(x=factor(season, levels=seas_ord), y=n, fill=season))
s + geom_bar(stat="identity", width = 0.7) +
 labs (x="Seasons", y="Detected Fires") +
 scale_fill_manual(values=c("#F77F00", "#D62828", "#FCBF49","#003049"),
          limits = c("spring", "summer", "fall", "winter")) +
 theme_bw() + theme(text = element_text(size = 18, family = "Calibri"), axis.text.x=element_text(size = 16, margin = margin(t = 1,
r = 1, b = 1, l = 1)),
     axis.text.y=element_text(size = 16,  margin = margin(t = 1, r = 1, b = 1, l = 1)),
```

```
    legend.position = "none") +
  scale_x_discrete(labels=c("fall" = "Fall", "spring" = "Spring",
                "summer" = "Summer", "winter" = "Winter"))
dev.off()

#Comparing with the total fires - 1496
tot<-read.csv("month_total.csv", header=TRUE, sep=";")
head(tot)
month_yes<-as.data.frame(images_yes %>% group_by(month) %>% tally())
df1<-data.frame(1,0)
names(df1)<-c("month","n")
df2<-data.frame(3,0)
names(df2)<-c("month","n")
df3<-data.frame(10,0)
names(df3)<-c("month","n")
df4<-data.frame(11,0)
names(df4)<-c("month","n")
df5<-data.frame(12,0)
names(df5)<-c("month","n")
month_yes<-rbind(month_yes, df1, df2, df3, df4, df5)
month_yes<-month_yes %>% arrange(month)

total_month<-cbind(tot, month_yes$n)
#total_month<-cbind(tot, month_yes$n, month_no$n)
#names(total_month)<-c("month", "n_total", "n_yes", "n_no")
names(total_month)<-c("month", "n_total", "n_yes")
head(total_month)

total_month$prop_yes<-round((total_month$n_yes * 100)/total_month$n_total,2)
#total_month$prop_no<-round((total_month$n_no * 100)/total_month$n_total,2)
write.csv(total_month, "_proportion.csv", row.names = FALSE)

#s<-total_month[,c("month", "prop_yes", "prop_no")]
s<-total_month[,c("month", "prop_yes")]

long <- as.data.frame(melt(setDT(s), id.vars = 1))

tiff(file = "02_proportion_fires_months.tiff", width = 3200, height = 1600, units = "px", res = 300)
s <- ggplot(long, aes(x = as.factor(month), y = as.numeric(value), fill=variable))
s + geom_bar(position = "dodge", stat="identity") +
  labs (x="Months", y="Proportion (%)") +
  scale_fill_manual(name = "Detected Fires", values=c("#003049","#003049"), labels = c("Yes", "No")) +
  theme_bw() + theme(text = element_text(size = 18), axis.text.x=element_text(size = 18,
                margin = margin(t = 20, r = 20, b = 20, l = 20)),
      axis.text.y=element_text(size = 16,
                margin = margin(t = 20, r = 20, b = 20, l = 20)))
dev.off()

#Comparing for season
long$season<-ifelse(long$month %in% 3:5, "spring", ifelse(long$month %in% 6:8, "summer",
                ifelse(long$month %in%9:11, "fall", "winter")))
head(long)

season<- as.data.frame(long %>%
                group_by(season, variable) %>%
                summarise(sum = sum(value)))

seas_ord<-c("spring", "summer", "fall", "winter")
```

```
tiff(file = "03_Fire_proportion_season.tiff", width = 3200, height = 1600,
    units = "px", res = 300)
s <- ggplot(season, aes(x = factor(season, levels=seas_ord), y = as.numeric(sum), fill=variable))
s + geom_bar(position = "dodge", stat="identity") +
 labs (x="", y="Proportion (%)") +
 scale_fill_manual(name = "Detection", values=c("#003049","#003049"), labels = c("Yes", "No")) +
 theme_bw() + theme(text = element_text(size = 18), axis.text.x=element_text(size = 18,
                    margin = margin(t = 20, r = 20, b = 20, l = 20)),
      axis.text.y=element_text(size = 16,
                    margin = margin(t = 20, r = 20, b = 20, l = 20))) +
 scale_x_discrete(labels=c("fall" = "Fall", "spring" = "Spring",
                "summer" = "Summer", "winter" = "Winter"))
dev.off()

#Simplifying
bookmelt<-read.csv("Book2.csv", header=T,sep=",")
bm<- as.data.frame(melt(setDT(bookmelt), id.vars = 1))

seas_ord<-c("spring", "summer", "fall", "winter")

tiff(file = "03_new_detected_.tiff", width = 3200, height = 1600,
    units = "px", res = 300)
s <- ggplot(bm, aes(x = factor(ï..season, levels=seas_ord), y = as.numeric(value), fill=variable))
s + geom_bar(position = "dodge", stat="identity") +
 labs (x="", y="Proportion (%)") +
 scale_fill_manual(name = "", values=c("#003049","#D62828"),
            labels = c("Total Fire", "Detected Fire")) +
 theme_bw() +
 theme(text = element_text(size = 18),
     axis.text.x=element_text(size = 16,
                    margin = margin(t = 20, r = 20, b = 20, l = 20)),
     axis.text.y=element_text(size = 16,
                    margin = margin(t = 20, r = 20, b = 20, l = 20))) +
 scale_x_discrete(labels=c("fall" = "Fall", "spring" = "Spring",
                "summer" = "Summer", "winter" = "Winter"))
dev.off()
```

APPENDIX V – R SCRIPT RESEARCH QUESTION 3

```
###Research Question 3###

# yes and no for dnbr
dnbr<-as.data.frame(images %>% count(dNBR_Id))
dnbr #46 yes / 42 no

# Difference in days from the images
images$datadif<-(images$Img_DATE_post - images$DATEAL)
images$dNBR_Id <- as.factor (images$dNBR_Id)
images_yes2 <- images %>% filter(dNBR_Id == "yes")
head(images_yes2)

# Ploting
tiff(file = "04_dnbr-diff.tiff", width = 3200, height = 3200,
    units = "px", res = 300)
g<- ggplot(images_yes2, aes(x=dNBR_Id, y=datadif, fill=dNBR_Id)) g +  geom_boxplot() +
  labs (x="", y="Difference (days)") + scale_fill_manual(values=c("#00507A", "#F77F00")) +
  theme_bw()+ theme(text = element_text(size = 18),
      axis.title = element_text(face="bold"),
      axis.text.x=element_text(size = 18, margin = margin(t = 1, r = 1, b = 1, l = 1)),
      axis.text.y=element_text(size = 16, margin = margin(t = 1, r = 1, b = 1, l = 1)),
      legend.position = "none")+ scale_x_discrete(labels=c("yes" = "Yes"))
dev.off()

# Violin Plot
tiff(file = "Ver03_05_violin_dnbr-diff2.tiff", width = 3200, height = 3200,
    units = "px", res = 300)
g<- ggplot(images_yes2, aes(x=dNBR_Id, y=datadif, colors=dNBR_Id))
g + geom_violin() + labs (x="", y="Difference (days)") + scale_color_manual(values=c("#D62828")) +
  geom_jitter(aes(colour = dNBR_Id), position = position_jitterdodge(dodge.width = 1.5), size=5) +
  theme_bw() +
  theme(text = element_text(size = 24), axis.text.x=element_text(size = 24,   margin = margin(t = 10, r = 10, b = 10, l = 10)),
      axis.text.y=element_text(size = 20,  margin = margin(t = 10, r = 10, b = 10, l = 10)),
      legend.position = "none") + scale_x_discrete(labels=c("yes" = "Detected Fires"))
dev.off()

# Checking count, max, min and mean
images$datadif<-as.numeric(images$datadif)
dnbr_dif<-data.frame(
  images %>% group_by(dNBR_Id) %>% tally(),
  images %>% group_by(dNBR_Id) %>% summarise(max = max(datadif)),
  images %>% group_by(dNBR_Id) %>% summarise(min = min(datadif)),
  images %>% group_by(dNBR_Id) %>% summarise(mean = round(mean(datadif),2)),
  images %>% group_by(dNBR_Id) %>% summarise(sd = round(sd(datadif),2)))
dnbr_dif <- dnbr_dif [ ,c("dNBR_Id", "n", "max", "min", "mean", "sd")]
dnbr_dif #vou salvar num csv para vc ter acesso rapido
#write.csv(dnbr_dif, "_dnbr_dif_stats.csv", row.names = FALSE)

# Statistical diffrence from the diffrences
images$datadif<-as.numeric(images$datadif)
shapiro.test(images$datadif) # not normal distribution
kruskal.test(datadif ~ dNBR_Id, data=images) # Significantly different (p=0.005)

# Conclusion: Time between the fire and the image, influences the detection

### Calculating the relation between the difference (Days) and the Total burned
```

```
head(images)
nrow(images)
burn_dif<-as.data.frame(images %>%
                group_by(dNBR_Id, datadif) %>%
                summarise(mean = mean(Burned_total)))
burn_dif <- burn_dif %>% filter(dNBR_Id == "yes")
head(burn_dif)
nrow(burn_dif)


tiff(file = "07_burn_dif_MEAN.tiff", width = 3200, height = 3200,
    units = "px", res = 300)
ggplot(burn_dif, aes(x=datadif, y=mean, color=dNBR_Id)) +
  geom_point() + labs (x="Difference (days)", y="Mean burned total area (ha)") +
  scale_color_manual(name = "Detection", values=c("#F77F00"), labels = c("Yes")) +
  geom_jitter(aes(colour = dNBR_Id), size=5) +theme_bw() + theme(text = element_text(size = 35),
      axis.text.x=element_text(size = 35,
                    margin = margin(t = 20, r = 20, b = 20, l = 20)),
      axis.text.y=element_text(size = 35,
                    margin = margin(t = 20, r = 20, b = 20, l = 20)))
dev.off()


### BURN DIF TOTAL REAL
images_burned_total <- images %>% filter(dNBR_Id == "yes")
head(images_burned_total)

tiff(file = "AMA2_08_burn_dif.tiff", width = 3200, height = 3200,
    units = "px", res = 300)
g<- ggplot(images_burned_total, aes(x=datadif, y=Burned_total, color=dNBR_Id))
g +  geom_point() + labs (x="Difference (days)", y="Burned total area (ha)") +
  scale_color_manual(name = "Detection", values=c("#FCBF49"), labels = c("Detected Areas")) +
  geom_jitter(aes(colour = dNBR_Id), position = position_jitterdodge(dodge.width = 0.1), size=7) +
  theme_bw() + theme(text = element_text(size = 20), axis.text.x=element_text(size = 18,  margin = margin(t = 10, r = 10, b = 10,
l = 10)),
      axis.text.y=element_text(size = 18,  margin = margin(t = 10, r = 10, b = 10, l = 10)))
dev.off()

shapiro.test(images$Burned_total) # not normal distribution
kruskal.test(Burned_total ~ datadif, data=images) # not sig. different (p=0.3)
```

60